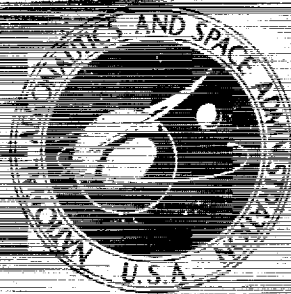


NASA TECHNICAL
MEMORANDUM



NASA TM X-3135

NASA TM X-3135

CASE FILE
COPY

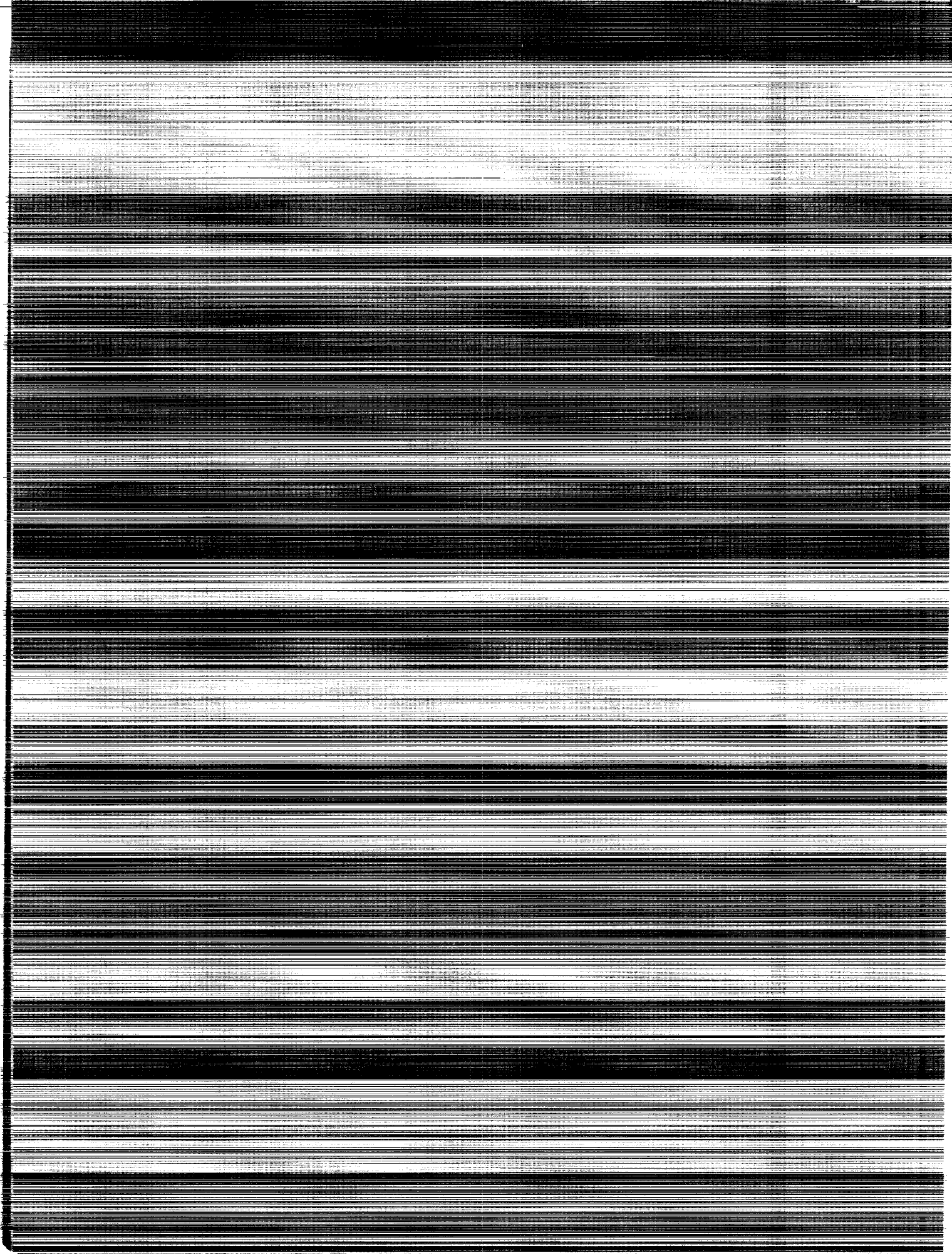
DESIGN OF A VERY-LOW-BLEED
MACH 2.5 MIXED-COMPRESSION INLET
WITH 45 PERCENT INTERNAL CONTRACTION

*Joseph F. Wasserbauer, Robert J. Shaw,
and Harvey E. Neumann*

*Lewis Research Center
Cleveland, Ohio 44135*



NATIONAL AERONAUTICS AND SPACE ADMINISTRATION • WASHINGTON, D. C. • MARCH 1975



1. Report No. NASA TM X-3135	2. Government Accession No.	3. Recipient's Catalog No.	
4. Title and Subtitle DESIGN OF A VERY-LOW-BLEED MACH 2.5 MIXED-COMPRESSION INLET WITH 45 PERCENT INTERNAL CONTRACTION		5. Report Date March 1975	6. Performing Organization Code
		8. Performing Organization Report No. E-8098	10. Work Unit No. 505-04
7. Author(s) Joseph F. Wasserbauer, Robert J. Shaw, and Harvey E. Neumann		11. Contract or Grant No.	
9. Performing Organization Name and Address Lewis Research Center National Aeronautics and Space Administration Cleveland, Ohio 44135		13. Type of Report and Period Covered Technical Memorandum	
		14. Sponsoring Agency Code	
12. Sponsoring Agency Name and Address National Aeronautics and Space Administration Washington, D. C. 20546		15. Supplementary Notes	
16. Abstract A full-scale, mixed-compression inlet was designed for operation with the TF30-P-3 turbofan engine and tested at Mach numbers of 2.5 and 2.0. The two-cone axisymmetric inlet had minimum internal contraction consistent with high total pressure recovery and low cowl drag. At Mach 2.5, inlet recovery was 0.906 with only 0.021 centerbody bleed mass-flow ratio and no cowl bleed. Increased centerbody bleed gave a maximum inlet unstart angle of attack of 6.85°. At Mach 2.0, inlet recovery was 0.94 with only 0.014 centerbody bleed mass-flow ratio and no cowl bleed. Inlet performance and angle-of-attack tolerance is presented for operation at Mach numbers of 2.5 and 2.0.			
17. Key Words (Suggested by Author(s)) Supersonic cruise inlets Inlets Propulsion systems		18. Distribution Statement Unclassified - unlimited STAR category 07 (rev.)	
19. Security Classif. (of this report) Unclassified	20. Security Classif. (of this page) Unclassified	21. No. of Pages 70	22. Price* \$4.25

* For sale by the National Technical Information Service, Springfield, Virginia 22151

DESIGN OF A VERY-LOW-BLEED MACH 2.5 MIXED-COMPRESSION INLET
WITH 45 PERCENT INTERNAL CONTRACTION

by Joseph F. Wasserbauer, Robert J. Shaw, and Harvey E. Neumann

Lewis Research Center

SUMMARY

The design and performance of a Mach 2.5 full-scale axisymmetric, bicone, mixed-compression inlet is presented. The inlet matched the airflow requirements of the TF30-P-3 turbofan engine at Mach 2.5 flight speeds. The design featured a short supersonic diffuser with a short cowl length from cowl lip to throat. The boundary layer that was generated on the cowl was thin and eliminated the need for cowl bleed at the throat. A slot bleed was used on the centerbody to provide boundary layer control at the high-pressure-gradient region on the centerbody. The region of high-pressure gradient was generated by nearly focusing the internal compression fan from the cowl and the cowl-lip shock on the centerbody. The study was conducted at Mach numbers of 2.5 and 2.0 at a Reynolds number of 8.2×10^7 per meter.

With a sealed bypass system at Mach 2.5, inlet pressure recovery was 0.906 with only 0.021 centerbody bleed mass-flow ratio and no cowl bleed. Variation of the centerbody bleed exit area provided additional stability range for subcritical operation. At Mach 2.0, inlet total pressure recovery was 0.94 with only 0.014 centerbody bleed mass-flow ratio. At Mach 2.5 operation and with a centerbody bleed mass-flow ratio of 0.02, the maximum inlet unstart angle of attack was 2.55° . Increasing the centerbody bleed mass-flow ratio to approximately 0.05 gave a maximum inlet unstart angle of attack of 6.85° . Over the inlet's operating range, steady-state distortions at 0° angle of attack varied from 6 percent to 11 percent at Mach 2.5 operation and from 8 percent to about 12 percent at Mach 2.0 operation. Inlet operation with an operating bypass system reduced the total pressure recovery slightly and increased the steady-state distortion.

INTRODUCTION

Supersonic inlets should be able to operate efficiently with low drag over the entire flight range of the aircraft. For flight speeds above Mach 2.0, mixed-compression inlets offer this capability. However, some means of varying the inlet's contraction ratio must be provided to supply engine airflow demands at flight speeds below the design Mach number.

Two-dimensional inlets provide this variation of contraction ratio by relatively simple movable ramp surfaces. The problem is more difficult, however, with axisymmetric designs. Single-cone axisymmetric inlets have been designed which vary the contraction ratio by either collapsing or translating the centerbody, or by collapsing the cowl and translating the centerbody (refs. 1 and 2). In general, these single-cone axisymmetric inlets have high internal contraction for the supersonic compression, which results in a fairly long diffuser. Consequently, a relatively high boundary-layer-bleed flow rate is necessary to provide the desired inlet performance at design flight speeds. Minimization of this performance bleed while maintaining inlet performance could improve the overall inlet drag characteristics. An alternate approach to this problem might be to decrease the amount of internal contraction in order to reduce the bleed drag. Although the resulting increase in cowl pressure drag may nullify this improvement in bleed drag, other characteristics (such as improved angle-of-attack tolerance) are obtained which may be desirable for certain mission applications.

In reference 3 an inlet with low internal contraction and a short supersonic diffuser showed reductions in performance bleed while maintaining relatively high pressure recovery. In addition, significant increases in angle-of-attack tolerance were also demonstrated. The inlet of reference 3 and the inlet presented herein were based on similar design philosophies. A two-cone spike was used to provide the maximum external compression compatible with high total pressure recovery and relatively low cowl drag (ref. 4). This design concept permits significant reduction of the supersonic diffuser length from cowl lip to inlet throat and thus reduces the amount of cowl bleed necessary at the throat. In order to vary contraction ratio for a flight inlet, the second cone would be collapsed, and at its lowest position it would blend into the first-cone contours so as to provide a single-cone centerbody. This philosophy provides 45 percent of the supersonic area contraction internally for a design Mach number of 2.5. This inlet was designed such that the isentropic com-

pression fan from the cowl and the cowl-lip oblique shock were nearly focused on the inlet's centerbody. This compression was canceled at the centerbody with a sharp turn, as prescribed by a computer program for the designing of inlets by an inviscid method of characteristics. A centerbody bleed slot was provided over this compression region for boundary layer control just ahead of the inlet throat. The slot bleed technique should provide relatively simple boundary layer control on the centerbody even in the partially collapsed positions. The relatively high pressure on the 18.5° second cone tended to reduce recirculation problems due to possible leakage in the collapsible surface. The inlet model is a full-scale design sized to provide airflow to a TF30-P-3 turbofan engine at a design Mach number of 2.5.

The inlet was tested at Mach numbers of 2.5 and 2.0. A second centerbody was designed as a collapsed version for Mach 2.0 operation. Flow surveys to evaluate local flow conditions were made in the inlet at the throat and throat exit stations, midway in the subsonic diffuser, and at the diffuser exit. In addition to the flow surveys, measurements were made of centerbody bleed flow rates, total pressure recovery, and engine face distortion. The maximum angle of attack before inlet unstart was determined for various inlet operating conditions. The effect of an overboard bypass system was also evaluated.

GENERAL MODEL CONSIDERATIONS

The model is a full-scale inlet sized to meet the airflow demands of the TF30-P-3 turbofan engine at Mach 2.5. It is a mixed-compression inlet with 55 percent of the supersonic area contraction occurring externally and 45 percent internally. Model hardware was designed to simulate the external contours and operating systems of an operational inlet wherever possible. Internal contours were considered appropriate for an operational inlet.

Installation of the inlet model in the 10- by 10-Foot Supersonic Wind Tunnel is shown in figure 1(a). For this investigation the inlet was coupled to a cold-pipe choked plug assembly. The nacelle cutaway, illustrating the cold-pipe installation, is shown in figure 1(b).

At the design Mach number of 2.5 and a free-stream temperature of 390 K, the TF30-P-3 requires a corrected airflow of 65.8 kg/sec. The inlet capture area was 0.7073 square meter. For these conditions the engine required 93 percent of the cap-

ture mass flow at a total pressure recovery of 91.5 percent. Of the remaining inlet mass flow, 5.5 percent was allotted for performance bleed, 1.0 percent was allotted for overboard bypass flow for terminal shock position control, and 0.5 percent was spilled over the cowl.

The essential features of the inlet design are shown in the isometric view of figure 2(a) and the cross-sectional view of figure 2(b). The inlet centerbody had a two-cone spike with the initial cone angle at 12.5° and the second cone angle at 18.5° . The cowl lip had a sharp radius of 0.038 cm, and the initial internal cowl angle was 2° . The external cowl angle was set at 5° to keep the cowl drag at a low value.

Control for the diffuser flow in the throat region was provided by cowl bleed, forward and aft of the geometric throat, and by a centerbody bleed slot ahead of the throat. Vortex generators were provided on the cowl and centerbody to prevent diffuser flow separation. Overboard bypass doors were used for terminal shock control. The centerbody was supported by four equally spaced hollow struts. Internal valves in each strut were used to control centerbody bleed flow. The inlet was restarted by translating the centerbody during the test.

DESIGN

Inlet Contours

The internal contours of the supersonic diffuser were determined by using the inviscid method of characteristics flow solution described in reference 5. The Mach 2.5 theoretical inviscid flow field is shown in figure 3. At the design Mach number of 2.5 the centerbody cone angles are 12.5° and 18.5° for the initial and second cones, respectively. The design cowl-lip-position parameter θ_1 is 26.4° . Computations shown include the flow field mesh and the cowl and centerbody Mach number distributions (figs. 3(a) and (b)). Local static to free-stream total pressure ratio distributions on the cowl and centerbody are shown in figures 3(c) and (d) for supersonic and subsonic conditions. The pressure ratio distributions for axial distances greater than $x/R_c = 2.8$ were obtained from the subsonic diffuser area distribution and quasi-one-dimensional flow analysis. The inviscid total pressure recovery at the throat ($x/R_c = 2.78$) before the inlet terminal shock was 0.982 at a throat Mach num-

ber of about 1.30. This yielded a theoretical normal shock recovery of 0.962. The inlet throat section ($2.78 < x/R_c < 3.2$) had an initial area diffusion of 1° equivalent conical expansion with a length equal to 4 hydraulic radii. For supercritical operation the Mach number varied from about 1.30 to about 1.33 through this section. At the throat exit ($x/R_c = 3.2$) a linear variation in flow angle was assumed between the two surfaces. The mean velocity vector was directed at the midannulus location at the compressor face in order to minimize subsonic diffuser turning.

The inlet design was such that the isentropic compression fan from the cowl and the cowl-lip oblique shock were nearly focused on the centerbody (fig. 3(e)). The cowl-lip shock and cowl compression fan were canceled at the centerbody with a sharp turn and a short length of contoured surface before the throat, as prescribed by the inlet design computer program (fig. 3(a)). A centerbody bleed slot replaced the short length of contoured surface over this compression region for boundary layer control ahead of the inlet throat. The slot bleed would permit a relatively simple geometry to be retained during collapse of the centerbody. The focused compression reduces significantly the supersonic diffuser length from cowl lip to inlet throat (0.38 cowl diameter at cowl-lip station) and thus reduces the amount of cowl bleed, if any, that may be required at the inlet throat.

In order to minimize the cost of this particular inlet model, the spike did not collapse but rather was translated to vary the internal contraction ratio during testing. Hence, a second centerbody was designed as a collapsed version for Mach 2.0 operation. Its initial cone angle was 12.5° and the second-cone angle was 14.5° . The characteristic solution for the collapsed version of the centerbody for Mach 2.0 operation is shown in figure 4. Figures 4(a) and (b) show the flow field mesh and the Mach number distributions on the cowl and centerbody. At the throat ($x/R_c = 2.78$) the Mach number varied from 1.19 on the cowl to 1.15 on the centerbody. For off-design operation, shock cancellation did not occur and shock reflections were present. The local static to free-stream total pressure ratios for the cowl and centerbody supersonic and subsonic conditions are presented in figures 4(c) and (d).

The internal flow area distributions for the Mach 2.5 and Mach 2.0 centerbodies are shown in figure 5. A quasi-one-dimensional flow analysis was used to design the subsonic diffuser. The one-dimensional flow area used was based on an assumption of a linear variation in flow angle between the two surfaces. The subsonic diffuser was designed for a linear variation of static pressure with axial distance. But

the geometry of the inlet struts modified the area distribution such that the pressure variation of the subsonic diffuser was not linear. The effect is more pronounced for the Mach 2.0 centerbody design. The subsonic diffuser length measured from the geometric throat was 1.5 inlet diameters. The diffusion area ratio was matched to the compressor face Mach number required for the TF30-P-3 turbofan engine at Mach 2.5 operation. This resulted in an equivalent conical diffusion angle of 10° for the subsonic diffuser during Mach 2.5 operation. The coordinates of the cowl and the Mach 2.5 and Mach 2.0 centerbodies are listed in table I.

Performance Bleed

In reference 3 the cowl shock and cowl compression fan were focused at one point on the centerbody. An abrupt turn on the centerbody was used to cancel reflected shocks. A flush slot bleed was positioned ahead of this focal point at the end of the second-cone contour. The local flow expansions from the slot and the large static pressure rise of the centerbody, caused by the focused shock - compression-fan system, gave less than desired control of the boundary layer at this point. By positioning the bleed slot behind the cowl shock impingement point, advantage could be taken of the higher surface static pressures to provide better bleed pumping characteristics and higher bleed pressure recoveries in the centerbody cavity. Because of the better bleed pumping characteristics, local boundary layer separations in this region could be minimized.

Details of the centerbody bleed slot are shown in figure 6. The slot extended from $x/R_c = 2.583$ to $x/R_c = 2.688$, a length of approximately 10 percent of the inlet radius. Entrance geometry configurations could be varied from a sharp dump to a sloping contour (fig. 6(a)). Flush slot and ram scoop arrangements could be used with both sharp and blunt lip trailing edges (figs. 6(a) to (d)). The ram scoops were designed to intercept 3 percent of the duct flow (based on inviscid flow calculations) ahead of the geometric throat. The centerbody bleed flow was ducted through the centerbody hollow support struts to the free stream.

Two regions of porous bleed were incorporated on the cowl surface (fig. 7). The forward cowl bleed region was located in a region opposite the centerbody slot and extended from $x/R_c = 2.556$ to $x/R_c = 2.770$. It was composed of 25 rows of 0.3175-cm-diameter holes located on centerlines 0.410 cm apart. Rows were staggered in a

60° pattern to prevent inducing any significant circumferential variations in boundary layer properties. The aft cowl bleed region extended from $x/R_c = 2.797$ (just downstream of the geometric throat) to $x/R_c = 3.105$. It was composed of 36 rows of 0.3175-cm-diameter holes located on centerlines which were 0.408 cm apart. Aft holes were also staggered in a 60° pattern. Nominal surface porosity of both bleed regions was 40 percent.

Cowl bleed flows were discharged overboard through slot exits located on the external cowl surface. Bleed exit areas could be changed from configuration to configuration but not remotely. Cowl exit areas were sized for 1.4, 2.7, and 5.5 percent of the cowl-lip area.

Inlet Support Struts, Strut Valves, and Overboard Bypass Doors

Details of the inlet support struts and strut valves are shown in figure 8. Figure 8(a) shows a cross-sectional view of the inlet through the strut region at approximately the maximum strut blockage. The circumferential location of the overboard bypass doors (two per quadrant) and the centerbody strut bleed valves are indicated. Centerbody bleed flow was ducted through the four equally spaced hollow support struts and throttled by the strut bleed valves. The flow then passed to the free stream through louvered panels.

The detailed geometry of the centerbody support struts is shown in figure 8(b). The maximum length of the struts extended over half of the subsonic diffuser length. The leading edge of each strut was blunt and inclined to the inlet centerline. At the cowl the radius of the strut leading edge was 2.06 cm and expanded to 4.59 cm at the centerbody. At the design Mach number the struts were sized to accommodate a maximum centerbody bleed flow rate of about 7 percent of the inlet capture mass-flow ratio at a centerbody duct pressure recovery of 20 percent.

The area distributions of the struts are shown in figure 8(c). Two area distributions are shown: one for the Mach 2.5 centerbody, and the other for the Mach 2.0 centerbody. The strut area distribution for the Mach 2.0 centerbody was greater because the collapsed version of the centerbody exposed more strut surface.

The details of the strut bleed valves are shown in figure 8(d). Each strut contained a bleed valve assembly at the cowl termination. A hydraulic rotary actuator rotated the vane through 90° from closed to a full-open area of 261.71 sq cm.

The inlet was also equipped with eight overboard bypass doors designed for high-frequency-control studies (ref. 6). The doors were hydraulically actuated slotted plates (fig. 9(a)). The bypass doors were positioned from $x/R_c = 4.50$ to $x/R_c = 5.53$ in the subsonic diffuser. The circumferential location of the doors is shown in figure 8(a).

The overboard bypass exit area was sized to remove 90 percent of the engine mass-flow ratio at design operation. The exit area was oversized to provide adequate protection for the engine during an inlet unstart for the engine-inlet compatibility tests. The diffuser bypass flow passed through the choked slotted plate to a plenum and then through a louvered panel to the free stream. Installation of an overboard bypass door and centerbody strut bleed valve is shown in figure 9(b). A complete detailed description of the bypass doors is presented in reference 7.

The inlet was tested with and without an operating inlet overboard bypass system. When bypass doors were not used, insert blanks replaced the bypass door assemblies so that smooth surfaces were maintained on the internal cowl from the cowl lip to the diffuser exit.

Vortex Generators

Vortex generators were used on the cowl and centerbody to inhibit flow separation. Details of the vortex generator design are shown in figure 10. These vortex generators were one-half of a NACA-0012 airfoil with the mean camber line of the airfoil as the parting line. The leading edge was rounded. Figure 10(a) gives the dimensions for the two alternate sets of generators that were available for installation on the cowl and the centerbody. Both sets of vortex generators were designed to have aspect ratios of 0.5. Vortex generators, identified as set I, were designed to have a height, or span of the airfoils, of 2.54 cm for both the cowl and centerbody. This is equal to about one-fourth of the Mach 2.5 inlet throat height. The cord was equal to 5.044 cm. The spacing-to-height ratio of the set I generators was 3.81 for the cowl and 3.83 for the centerbody. This spacing nearly satisfied the complete mixing criterion of reference 8.

For vortex generator set II the span of the airfoils was 2.03 cm for the centerbody and 1.52 cm for the cowl. The cord was equal to 4.064 cm for the centerbody and 3.048 cm for the cowl. The spacing-to-height ratio was 2.40 for the centerbody and

3.18 for the cowl. Airfoil spacing for the cowl and centerbody vortex generators of set II satisfied the complete mixing criteria of reference 8.

Figure 10(b) shows the relative location of the generators with respect to the struts on both the cowl and centerbody. The same number of generators were used on both the Mach 2.5 and Mach 2.0 centerbodies. The vortex generators were located at $x/R_c = 3.37$ on the cowl and on each centerbody. The inlet performance reported herein includes only the set II generators. The performance of the inlet operating with both sets of generators is presented in reference 9.

Model Instrumentation

The diffuser exit or engine mass-flow ratio was calculated by using a calibrated choked plug and an average of eight static pressure taps in the cold pipe located 5.78 cowl-lip radii (radius of the cowl at the cowl lip) ahead of the plug exit (fig. 1(b)). Cowl bleed flow rates at both the forward and aft cowl locations were determined from three circumferentially positioned static and total pressure surveys at their respective exits and the measured exit areas (fig. 7). The centerbody bleed mass-flow ratio was determined from the measured total pressures in the centerbody duct and hollow support struts (fig. 8(a)), the strut valve choked exit area, and an experimentally determined flow coefficient.

In order to calculate the overboard bypass mass-flow ratio, an assumption was made that the average main-duct static pressure spanning the bypass door region was equal to the total pressure ahead of the calibrated choked bypass exit. The average main-duct static pressure spanning the bypass door region was determined from rows of four static pressure taps circumferentially located at 0° , 90° , and 180° (fig. 8(a)). The average static pressure for each row was used as the total pressure for the adjacent bypass doors. Static pressures at the circumferential location of 270° were assumed to be equal to the 90° circumferential location because of flow symmetry. The centerbody bleed flow was surveyed at the slot entrance for the flush slot and ram scoop configurations by measurements of static and total pressure, as indicated in figure 11.

The static pressure variation throughout the inlet was determined from static pressure taps located along the top centerline of both the cowl and centerbody. Additional static pressure taps were located at 180° from the top centerline on both the

cowl and centerbody. The locations of all the static pressure taps are listed in table II for the cowl and both the Mach 2.5 and Mach 2.0 centerbodies.

The inlet flow was surveyed by total pressure probes at the throat and the throat exit, midway in the subsonic diffuser, and at the diffuser exit. The boundary layer on the cowl and centerbody at the throat was surveyed by the probes illustrated in figure 12(a). The details of the total pressure rakes at the mid-diffuser and throat exit locations for the two centerbodies are shown in figures 12(b) and (c). The rakes were circumferentially indexed to avoid mutual interference effects.

The details of the steady-state total and static pressure instrumentation at the compressor face are shown in figure 12(d). The overall diffuser exit total pressure recovery was determined from rakes 1 to 12, which had six area-weighted tubes per rake. Rakes 1, 7, and 10 had three additional total pressure probes to better define the boundary layer on the cowl and centerbody at the diffuser exit. The angular location of the 12 rakes has been adjusted for the presence of the four struts. This resulted in a 2.5° correction on 8 of the 12 rakes adjacent to the struts. Wall static pressure measurements were made with the 20 wall static pressure taps shown in figure 12(d).

In order to measure the fluctuating component of total pressure, subminiature absolute pressure transducers were mounted in the rakes at the three locations shown in figure 12(d). The transducers were mounted in the rakes such that a simultaneous steady-state and dynamic pressure measurement could be made. The resultant configuration provided a flat response to at least 1000 hertz. The output signal was passed through a second-order low pass filter with a 1000-hertz corner frequency and was measured with a true rms meter. The filtered fluctuating component of each pressure transducer was also recorded on frequency-modulated magnetic tape.

At each steady-state operating condition, dynamic data were recorded at each of the three locations shown in figure 12(d). The average value of the associated rms measurements of the fluctuating component of total pressure was ratioed to the average steady-state total pressure recovery. This average value is defined herein as the dynamic distortion level for that particular operating condition.

Configuration and Test Procedure

A number of inlet operating conditions were investigated for the design Mach 2.5

centerbody configuration and for the collapsed version of the centerbody at Mach 2.0. Regions of cowl bleed were provided at the inlet throat. The cowl bleed evaluation study showed that the increased performance did not offset the increased cowl bleed drag. Therefore, these bleed regions were sealed for data presented herein. The flush slot with the dump leading edge and a blunt lip trailing edge (fig. 6(b)), proved to be the most efficient slot geometry during the centerbody bleed evaluation study. This report presents the data for this configuration only.

Data were obtained for peak, subcritical, critical, and supercritical operation. Peak operation is defined as the minimum stable condition with the terminal shock at its most forward position in the inlet before an inlet unstart occurs. At 0° angle of attack, this operating condition occurs for subcritical operation only. Operation with the terminal shock between the throat and the most forward position is defined to be subcritical operation. Critical operation is defined as operation with the terminal shock positioned at the inlet's geometric throat. Supercritical operation is hence defined as operation with the terminal shock downstream of the throat.

At the inlet design Mach number and contraction ratio and at 0° angle of attack, a centerbody bleed flow rate was determined to obtain the maximum total pressure recovery for critical inlet operation. This centerbody bleed flow rate is referred to herein as the optimum centerbody bleed flow rate. Data were also obtained for values of centerbody bleed flow rate greater than optimum for all inlet operating conditions.

During angle-of-attack operation a minimum stable operating condition (peak) was determined for subcritical, critical, and supercritical inlet conditions. At angle-of-attack operation, minimum stable conditions were determined for the optimum and increased centerbody bleed flow rates. These angle-of-attack data are referred to as maximum angles of attack.

The inlet was tested with a sealed bypass system and an operating bypass system. At the inlet design Mach number and contraction ratio, and with the bypass system sealed, 0° angle-of-attack data were taken at various compressor face corrected airflows by varying the main-duct exit area. With the bypass system operating, data were taken for various overboard bypass flows. The match compressor face corrected airflow required for the TF30-P-3 was maintained for this data with a constant main-duct exit area.

RESULTS AND DISCUSSION

Inlet Performance without Bypass Flow

The inlet performance for Mach 2.5 and Mach 2.0 operation with a sealed bypass system is shown in figure 13. The data were obtained over a range of compressor face engine airflows by varying the main-duct choked plug exit area. Presented is the pressure recovery as a function of inlet bleed mass-flow ratio, steady-state distortion, and dynamic distortion. With a sealed bypass system, inlet performance is sensitive only to the amount of performance bleed. Therefore, the variation of bleed mass-flow ratio as a function of total pressure recovery is presented, rather than the conventional engine mass-flow ratio. The inlet of this investigation was designed to spill 0.5 percent of the inlet capture mass flow over the cowl at Mach 2.5 operation. The engine mass-flow ratio was then the inlet capture mass-flow ratio, 0.995, minus the inlet bleed flow, when the overboard bypass system was not installed. Steady-state distortion is defined as the maximum total pressure minus the minimum total pressure divided by the average total pressure. An average rms value of the fluctuating component of the total pressure was obtained for the three dynamic probes.

At the design free-stream Mach number of 2.5 the inlet pressure recovery was 0.895 at a bleed mass-flow ratio of 0.019 for critical operation. The maximum pressure recovery (peak) was 0.906 at a bleed mass-flow ratio of only 0.021 for subcritical operation, representing a minimum stable condition. The centerbody bleed exit area (strut butterfly flow area) was maintained constant for all data represented by open symbols in figure 13. The stable subcritical range for this centerbody bleed exit setting was about 1 percent. This was probably due to the absence of any cowl bleed and the relatively low centerbody bleed. The stable subcritical range for this inlet is defined as the percentage change in engine corrected airflow between critical operation and the minimum stable condition.

The stable subcritical range of the inlet with increased centerbody bleed is indicated by the solid symbols in figure 13. The inlet bleed mass-flow ratio was varied by changing the bleed exit area by means of the strut butterfly valves. With the maximum bleed exit area available, an additional 3 percent of the inlet capture mass-flow ratio was removed before the inlet unstated. This represents a stable subcritical range of 6 percent. Peak inlet pressure recovery during this subcritical operation was 0.915.

Steady-state distortion varied from about 6 percent to 11 percent over the operating range presented in figure 13. At 0° angle of attack the distortion was primarily radial at all terminal shock positions. Dynamic distortion remained about 2 percent over the range of inlet operation. However, the dynamic activity was measured at only three total pressure probe locations at the diffuser exit plane and in regions of low radial velocity gradients. The dynamic activity over the remainder of the diffuser exit plane was to be measured in a subsequent test. In general, the level of dynamic activity appeared to be acceptable for operation at the Mach 2.5 condition.

Inlet performance for the simulated collapsed version of the centerbody at Mach 2.0 is shown in figure 13(b). Peak inlet pressure recovery for the fixed bleed exit area was 0.940 with only 0.014 bleed mass-flow ratio. Inlet capture mass-flow ratio at Mach 2.0 was 0.918, and the remainder was spilled around the cowl through the spike shock systems (fig. 4(a)). Increasing the centerbody bleed exit area increased the bleed mass-flow ratio to 0.045. The peak recovery was 0.948 at a bleed mass-flow ratio of 0.035. The stable subcritical range was 4 percent for operation at a free-stream Mach number of 2.0. Steady-state distortion varied from 0.085 to 0.125 over the inlet operating range. For the increased bleed the distortion remained low at about 0.085. Dynamic distortion remained at about 1.0 percent over the range of inlet operation at Mach 2.0.

Performance with Bypass Flow

The inlet's performance at Mach 2.5 when the overboard bypass system was operating is presented in figure 14. Here, engine mass-flow ratio was directly affected by both centerbody bleed and bypass mass-flow ratio. Therefore, inlet performance is presented as a function of engine mass-flow ratio rather than of just the centerbody bleed mass-flow ratio. With the bypass doors closed, the leakage mass-flow ratio through the bypass doors was 0.009 of the inlet capture mass-flow ratio. In figure 14(a) the circular data points represent the inlet's performance with the bypass doors closed when the engine face corrected airflow was varied. The square data points represent variation of the bypass flow at a constant engine corrected airflow of 70.5 kg/sec. The peak pressure recovery with the bypass doors closed was 0.888 at a centerbody bleed mass-flow ratio of 0.02. The peak pressure recovery for the increased centerbody bleed flow was 0.906. Inlet distortion varied from 12 percent to

16 percent over the inlet operating range .

Peak pressure recovery for optimum centerbody bleed ($m_{b1}/m_0 = 0.02$) was 0.892 when the overboard bypass flow was set for 0.067 mass-flow ratio (fig. 14(b)). This bypass flow was necessary to match the TF30-P-3 engine corrected airflow demand of 65.8 kg/sec at the Mach 2.5 flight speed for critical inlet operation . For centerbody bleed flow rates larger than optimum the peak recovery was 0.911. The steady-state distortion ranged from 0.10 to 0.16 over the inlet operating range . In both instances for the operating bypass system , inlet performance was less than when the insert blanks replaced the bypass door assemblies . This implies that with leakage or bypass flow , the presence of the exit bypass ports creates large-scale surface effects that result in increased loss in total pressure recovery . These surface effects also tended to reduce the pressure gradients near the wall such that the flow was near separation . This will be pointed out in later figures . The dynamic distortions , which were obtained by varying either the bypass flow or the exit plug area , were similar at comparable levels of recovery for critical and supersonic shock positions .

The stability performance and bleed characteristics of the centerbody bleed system are presented in figure 15. The various symbols represent different bleed exit areas . Open symbols represent the minimum subcritical flow just before unstart where the highest inlet and bleed recoveries are obtained . The solid symbols on the bleed plot represent the supersonic bleed conditions . The solid symbols on the inlet performance curve represent the maximum recovery corresponding to the supersonic bleed flow . Stable operating margin could be obtained for this inlet by opening the centerbody bleed exit area from the optimum value of 16.3 percent ($m_{b1}/m_0 = 0.02$) to 86.5 percent .

The stability characteristics of the bleed system would be used only when some inlet flow disturbance would cause the terminal shock to move forward of the throat and unstart the inlet . A control system would be needed which employs the full capacity of the bleed system . An active control appears to be a feasible design . This control would provide full bleed exit area and maximum bleed mass-flow ratio upon command from a control signal , such as a step change in throat Mach number .

In reference 10 a cowl stability bleed system was demonstrated that would not be activated unless the terminal shock moved forward of the inlet throat . Perhaps a similar system could be devised for the centerbody bleed system .

Inlet performance over an angle-of-attack range is shown in figure 16. The following procedure was used to obtain the maximum angle-of-attack data for optimum and increased centerbody bleed flow rates. For maximum angle of attack at critical inlet operation, (1) the inlet was set at the critical operating point for 0° angle of attack, and (2) the model angle of attack was increased until an unstart occurred. The inlet was restarted, and data were then recorded for an angle slightly less than the unstart angle of attack. This angle-of-attack point is a minimum stable condition for critical inlet operation. Determination of the maximum angle of attack for peak inlet operation (minimum stable condition) follows the same procedure as for critical operation.

For maximum angle of attack at supercritical inlet operation (1) the inlet mass-flow plug was fully retracted; (2) the model angle of attack was increased until an unstart occurred; (3) the inlet was restarted and the model angle of attack was set slightly less than the unstart angle; (4) the mass-flow plug was then closed until the inlet unstarted; and (5) after the inlet was restarted, the plug was relocated near the position causing unstart. This data point is defined as the minimum stable condition for supercritical inlet operation. For angle-of-attack operation with increased centerbody bleed flow the same procedure was used for peak (subcritical), critical, and supercritical inlet operation. The angle-of-attack operation is presented for both optimum and maximum centerbody bleed exit areas. For optimum centerbody bleed mass-flow ratio the maximum supercritical angle of attack was 2.55° . For critical inlet operation, that is, with the terminal shock in the throat, the angle of attack before an inlet unstart was 1.74° . Increasing the centerbody bleed strut valve exit area to allow for maximum centerbody bleed flow resulted in angles of attack of 0.6° , 4.17° , and 6.85° for peak, critical, and supercritical operating conditions, respectively.

Steady-state distortion was 0.305 at an angle of attack of 6.85° . Although the inlet demonstrated a relatively large angle-of-attack range when centerbody bleed was increased, distortion may be a limiting factor. Consideration of the useful angle-of-attack range of any inlet must include the distortion sensitivity of the particular engine to which it is coupled.

For Mach 2.0 operation the maximum attainable angles of attack were 1.95° and 3.1° for optimum and maximum centerbody bleed, respectively. The recovery was 0.93 at a centerbody bleed mass-flow ratio of 0.031 for maximum centerbody bleed. With the optimum centerbody bleed the steady-state distortion during angle-of-attack operation was about the same at Mach 2.0 and Mach 2.5.

Diffuser Static Pressure Distributions

Flow variations as determined by measurements of the static pressure are given in figure 17 for operation at a free-stream Mach number of 2.5. Peak, critical, and supercritical terminal shock positions are shown for both the cowl and centerbody. Distributions are given for a sealed bypass and for two values of bypass flow at optimum centerbody bleed flow rates. Static pressure distributions for $x/R_c < 2.5$ agree well with the theoretical distribution. There was an overpressure on the centerbody at $x/R_c = 2.57$ due to the cowl shock impinging ahead of the cone shoulder. The sketch of figure 17(g) is an attempt to explain the forward intersection of the cowl shock ahead of the cone shoulder. The theoretical solution assumed that the cowl shock emanates from a sharp cowl lip and intersects the cone shoulder. However, the actual cowl lip had a radius of 0.038 cm. For supersonic flow the cowl shock was not attached but stood off a distance of about 0.06 cm. The inlet design did not account for the stand-off shock. The resulting shock structure at the cowl lip may be similar to that reported in reference 11. Hence, the cowl shock cancellation on the centerbody was not met.

The effect of the vortex generators at $x/R_c = 3.37$ can be seen in figure 17 as an increase in p/P_0 , followed by a decrease over a short range. This decrease was caused by a loss in recovery due to the vortex generators and is present in the cowl and centerbody distributions (figs. 17(a) and (b)) for the three terminal shock positions shown. Distributions with overboard bypass flow are similar to the distributions without bypass flow (figs. 17(c) to (f)). The distributions all show the characteristic of the loss in recovery due to the vortex generators and the resulting loss in p/P_0 throughout the subsonic diffuser. However, as indicated in reference 9, operation without vortex generators resulted in flow separation in the diffuser and an overall pressure recovery lower than when vortex generators were used. Similar results for Mach 2.0 operation are shown in figure 18. Again the vortex generators caused a reduction in the level of the pressure ratio.

Diffuser Performance

Distributions of local recovery profiles are shown in figure 19 for Mach 2.5 operation and in figure 20 for Mach 2.0 operation. Pressure profiles are presented for

the throat, throat exit, mid-diffuser, and diffuser exit locations. The individual tube pressures are uncorrected and represent the actual measured total pressure. The total pressures are normal shock pressures or that pressure behind the terminal shock, depending on the relative location of the inlet's terminal shock to the throat and throat exit rakes.

Boundary layer bleed on the cowl can be minimized or eliminated only when the boundary layer is sufficiently healthy and not near separation. For the inlet configuration tested and reported herein, no cowl bleed was used. The boundary layer profiles on the cowl for various inlet operating conditions at Mach 2.5 are compared in figure 19. For critical inlet operation the boundary layer height at the throat was only about 5 percent of the local duct height (fig. 19(b)). The supersonic diffusion on the cowl was moderate for the short cowl length (Mach number diffuses from 1.8 at the cowl lip to 1.3 at the throat), and hence the boundary layer growth was also moderate (fig. 19(b)). The incompressible shape factor of the measured cowl throat boundary layer was about 1.45 for critical operation. This indicates that the flow in the boundary layer at this point was not near separation. (A shape factor of about 1.8 would indicate boundary layer separation problems.) Further, the measured displacement thickness at the throat was in good agreement with analytical predictions. After the terminal shock the boundary layer grew to slightly more than 10 percent of the local duct height at the throat exit station.

With the terminal shock positioned upstream of the inlet throat (peak inlet operation), the severe adverse pressure gradient encountered on the cowl (fig. 17(b)) resulted in a throat boundary layer on the cowl of about 10 percent of the duct height (fig. 19(a)). The boundary layer grew to slightly more than 10 percent of the duct height at the throat exit station. Comparison of the boundary layer profiles at the throat exit on the cowl for peak and critical inlet operation shows the boundary layer heights to be nearly the same (figs. 19(a) and (b)). At the throat exit, no boundary layer separation was apparent for both inlet operating conditions. With vortex generators positioned just downstream of the throat exit, boundary layer separation problems in the diffuser should be eliminated. These results fortify the design philosophy that by shortening the supersonic diffuser, minimization or elimination of the cowl bleed can result. The normal shock recoveries in the inviscid core near the cowl at the throat station corresponded to the predicted value of 0.96 (figs. 19(b) and (c)).

On the centerbody, after the cowl shock intersection, the supersonic diffusion was

accomplished over a very short length and resulted in a large pressure gradient over this length. However, the centerbody bleed slot was positioned at this point to control the boundary layer. The expansion of the flow into the centerbody bleed slot readjusted the Mach number distribution near the slot. The flow was also redirected into the centerbody rather than parallel to it because of this flow expansion. As a result, additional shock losses were encountered on the centerbody. Figures 19(a) and (b) show that the total pressure losses near the centerbody at the throat were greater for peak inlet operation than for critical inlet operation. The reason was that at peak operation, the losses occurred in a higher Mach number flow region ahead of the throat where diffusion was not yet complete. At the throat exit station, these losses appeared as increased boundary layer growth on the centerbody.

Downstream of the throat the pressure distributions of figure 17(b) show that there was an adverse gradient at critical operation on the cowl as a result of the terminal shock. This adverse gradient resulted in a rapid increase in the viscous losses near the wall at the throat exit (fig. 19(b)). At the throat exit the static pressure distributions (fig. 17(b)) have similar values of diffusion; the recovery profiles for peak and critical operation should reflect this similarity. The throat exit profiles on the cowl (figs. 19(a) and (b)) were nearly the same. From the throat exit to the diffuser exit the static pressure diffusion was similar for peak and critical operation (figs. 17(a) and (b)). This led to the qualitative agreement shown in the recovery profiles at the diffuser exit (figs. 19(a) and (b)). Comparison of the throat exit and mid-diffuser profiles near the centerbody indicates that the vortex generators energized the flow. At the diffuser exit, fairly uniform profiles were measured. It appears that the vortex generators minimized any flow problems that might have occurred on the cowl and centerbody (ref. 9).

Total pressure recovery profiles for operation at a supercritical terminal shock position are shown in figure 19(c). The static pressure distributions for critical and supercritical operation were identical on the centerbody and cowl up to the throat (figs. 17(a) and (b)). Hence, the recovery profiles at the throat were identical at critical and supercritical operation. For this supercritical operating condition the terminal shock was just downstream of the throat exit station. The throat exit rake then displayed the supersonic profile at this station. Theoretical recovery was 0.957 at this station. The data indicated that the main stream met this recovery. In addition the flat profile indicated low total pressure distortions ahead of the terminal shock. At the mid-diffuser and diffuser exit rakes the profiles were similar to those

at critical inlet operation. But the profiles reflected lower recoveries because of the supercritical terminal shock position.

At Mach 2.5 operation the overall loss in total pressure recovery was 10 percent for critical inlet operation. Up to the throat station the 4 percent loss in total pressure in the inviscid core of the supersonic diffuser matched the theoretical predictions (fig. 19(b)). However, the average area-weighted total pressure recovery would be somewhat greater than the 4 percent because of boundary layer growth. The average area-weighted total pressure recovery for the throat exit rake was 0.93. Therefore, an overall loss in total pressure recovery of 7 percent had occurred up to the throat exit station. The additional 3 percent loss occurred in the subsonic diffuser downstream of the throat exit. No attempt was made to determine where or what part of this loss was due to viscous effects. Potential improvements in the subsonic diffuser (throat to diffuser exit station) to minimize pressure recovery loss and distortion are possible by redesigning the inlet struts, recontouring the subsonic diffuser walls, and improving the centerbody bleed slot geometry.

At Mach 2.0 operation the pressure distribution shown in figures 18(a) and (b) indicate that the terminal shock lay slightly upstream of the throat for peak and critical operation. The resultant distributions are hence similar. This similarity in diffusion and static pressure gradients resulted in essentially identical recovery distributions throughout the inlet for peak and critical operation (figs. 20(a) and (b)). For supercritical operation at Mach 2.0 the distributions of static pressure indicate moderate diffusion and pressure gradients through the throat exit as reflected in high recovery (fig. 20(c)). Between the throat exit and the mid-diffuser the terminal shock system resulted in a region of large recovery loss which was reflected in the distributions at the mid-diffuser and diffuser exit.

Diffuser Exit Recovery Profiles

Recovery profiles at the diffuser exit for critical inlet operation are shown in figures 21 and 22. Diffuser exit profiles without an operating overboard bypass system are shown in figure 21. Radial and circumferential distortions were small. Total pressure rake profiles for the top quadrant at critical inlet operation for an operating overboard bypass system are shown in figure 22. Only one quadrant is shown, but it was representative of the other quadrants because of symmetry. Figure 22(a) shows

the profiles for 0.009 bypass mass-flow ratio, and figure 22(b) for 0.068 bypass mass-flow ratio. A comparison of figure 21(a) and figures 22(a) and (b) shows that the center rake (rake 1) profile was essentially the same with or without bypass operation. However, the two side rakes, rake 12 and rake 2, in figures 22(a) and (b) showed tendencies for the flow to separate on the cowl when the bypass was operating. The result was a reduction in pressure recovery and an increase in steady-state distortion when the inlet bypass system was operating.

Rakes such as rake 12 and rake 2 measured the flow over the bypass door entrance slots. The entrance slots covered about the last one-third of the diffuser length and were located in the region of rapid area variation. The slot entrance of the bypass doors provided an abrupt increase in diffuser area of about 10 percent. This abrupt area change occurred repeatedly (8 times) over the length of the bypass door. The apparent large-scale roughness in a region of rapid area variation could tend to separate the flow, at least locally, as indicated by the comparison of rakes 2 and 12 with rake 1 which was located between the doors. Although bypassing the flow has the effect of delaying separation, the surface roughness may have had a greater effect on the local flow.

The diffuser exit profiles for critical inlet operation at a free-stream Mach number of 2.0 are shown in figure 23. The data presented are for operation without an overboard bypass system. The total pressure profiles indicate a region of high recovery at midpassage. This increased the radial distortion content; however, there was little circumferential distortion.

Distortion contours for typical operating conditions at Mach 2.5 and Mach 2.0 are shown in figure 24. The contour maps are a result of a computer program which uses the total pressure inputs at the diffuser exit. The solid lines on the contour plots show the position of the struts. At all operating conditions at 0° angle of attack, the contour maps show predominantly radial distortion with only small amounts of circumferential distortion.

Figure 25 shows the compressor face contours maps for the various angle-of-attack data presented in figure 16(a). For low angles of attack, up to about 2° , the distortion appeared to be more radial than circumferential. The circumferential distortion increased as the angle of attack was increased beyond 2° . At large angles of attack, low recovery regions appeared on the windward side, while relatively high recovery existed on the leeward side.

Comparison of Experimental and Theoretical

Subsonic Diffuser Performance

The performance of the subsonic diffuser is compared with theoretical predictions in figure 26. The performance was predicted with an axisymmetric viscous finite difference computation based on mixing theory (ref. 12). This theory was not available at the time the inlet was designed. The method of calculation in reference 12 does not account for the presence of the vortex generators and hence does not account for the losses associated with them. In figure 26(a) the theoretical static pressure distribution agrees well with the experimental data up to the axial location of the vortex generators. Beyond the vortex generators only qualitative agreement was obtained. The termination of the theoretical curve at $x/R_c = 4.6$ indicates the point of flow separation for the diffuser without vortex generators. This is in the region of the struts, or about the mid-diffuser location.

The theoretical flow profile at the mid-diffuser rake location indicates separated flow (fig. 26(b)). Because the centerbody vortex generators energized the flow, no separation was observed. However, comparison with data from reference 9 (where no vortex generators were used) shows good agreement with the theory. The predicted profile at the throat exit is also shown in figure 26(b). Fair agreement was obtained except near the centerbody. This can be attributed to the centerbody bleed slot recovery losses due to flow expansion into the bleed slot.

SUMMARY OF RESULTS

A full-scale, mixed-compression inlet sized for the TF30-P-3 turbofan engine was designed, and an experimental investigation was conducted at Mach 2.5 and Mach 2.0 operating conditions. The two-cone axisymmetric inlet had minimum internal contraction consistent with high total pressure recovery and low cowl drag. The following main results were drawn from this investigation:

1. At Mach 2.5 the maximum total pressure recovery with only 0.02 centerbody bleed mass-flow ratio and no cowl bleed was 0.906. At critical operation the total pressure recovery was 0.895 with only 0.019 centerbody bleed mass-flow ratio and no cowl bleed. Hence, this inlet compares favorably with similar high-performance

inlets which have lower cowl drag but greater bleed drag. At Mach 2.0 the inlet total pressure recovery was 0.94 with only 0.014 centerbody bleed mass-flow ratio for subcritical minimum stable operation.

2. At Mach 2.5 operation the stable subcritical range was increased from a value of 1 percent to 6 percent when the full capacity of the centerbody bleed system was used during subcritical operation.

3. At Mach 2.5 operation and with the minimum centerbody bleed mass-flow ratio of 0.02, the maximum unstart angle of attack for the inlet was 2.55° . Increasing the centerbody bleed mass-flow ratio to approximately 0.05 gave a maximum inlet unstart angle of attack of 6.85° .

4. Inlet steady-state distortions varied from 6 percent to 11 percent for Mach 2.5 operation and from 8 percent to about 12 percent for Mach 2.0 operation.

5. Diffuser total pressure profiles on the cowl at the inlet throat and throat exit stations showed acceptable boundary layer profiles at the various operating conditions without the benefit of cowl bleed. The 4 percent loss in total pressure in the inviscid core of the supersonic diffuser flow matched the theoretical predictions.

6. The overall loss in total pressure recovery was about 10 percent. Of this loss, 7 percent occurred up to the throat exit station and 3 percent in the subsonic diffuser. Inlet operation with an operating bypass system also reduced the total pressure recovery slightly and increased the steady-state distortion.

Lewis Research Center,

National Aeronautics and Space Administration,

Cleveland, Ohio, October 15, 1974,

505-04.

APPENDIX - SYMBOLS

A	flow area
A_c	capture area, 0.7073 sq m
d	height from surface to center of total pressure tube, m
H	annulus height at local diffuser station, m
h	distance from surface, m
M	Mach number
m/m_0	mass-flow ratio
P	total pressure, N/sq m
ΔP	fluctuating component of total pressure, N/sq m
p	static pressure, N/sq m
R_c	inlet capture radius, 0.4745 m
r	radius, m
x	axial location, m
θ_l	cowl-lip-position parameter, $\arctan (R_c/x)$, deg
φ	circumferential rake position, deg

Subscripts:

bl	centerbody bleed
by	bypass
max	maximum
min	minimum
rms	root-mean-square value
x	local
0	free stream
5	diffuser exit station

Superscript:

$(\bar{\quad})$ area-weighted average

REFERENCES

1. Smeltzer, Donald B.; and Sorensen, Norman E.: Tests of a Mixed Compression Axisymmetric Inlet With Large Transonic Mass Flow at Mach Numbers 0.6 to 2.65. NASA TN D-6971, 1972.
2. Koncsek, J. L.; and Syberg, J.: Transonic and Supersonic Test of a Mach 2.65 Mixed-Compression Axisymmetric Intake. NASA CR-1977, 1972.
3. Wasserbauer, Joseph F.; and Choby, David A.: Mach 2.5 Performance of a Bi-cone Inlet With Internal Focused Compression and 40-Percent Internal Contraction. NASA TM X-2294, 1971.
4. Wasserbauer J. F.; Shaw, R. J.; and Neumann, H. E.: Minimizing Boundary Layer Bleed for a Mixed Compression Inlet. AIAA Paper 73-1270, Nov. 1973.
5. Anderson, Bernard H.: Design of Supersonic Inlets by a Computer Program Incorporating the Method of Characteristics. NASA TN D-4960, 1969.
6. Baumbick, Robert J.; Wallhagen, Robert E.; Neiner, George H.; and Batterton, Peter G.: Dynamic Response of Mach 2.5 Axisymmetric Inlet With 40 Percent Supersonic Internal Area Contraction. NASA TM X-2833, 1973.
7. Webb, John A., Jr.; Mehmud, Oral; and Hiller, Kirby W.: Improved Design of a High-Response Slotted-Plate Overboard Bypass Valve for Supersonic Inlets. NASA TM X-2812, 1973.
8. Taylor Harland D.: Application of Vortex Generator Mixing Principles to Diffusers. R-15064-5, United Aircraft Corp., 1948.
9. Neumann, Harvey E.; Wasserbauer, Joseph F.; Shaw, Robert J.: Performance of Vortex Generators in a Mach 2.5 Low-Bleed Full-Scale 45-Percent Internal Contraction Axisymmetric Inlet. NASA TM X-3195, 1975.
10. Sanders, Bobby W.; and Mitchell, Glenn A.: Increasing the Stable Operating Range of a Mach 2.5 Inlet. AIAA Paper 70-686, June 1970.
11. Shapiro, Ascher H.: The Dynamics and Thermodynamics of Compressible Fluid Flow, Volume II. The Ronald Press Co., 1954, p. 1144.
12. Anderson, O. L.: Finite-Difference Solution for Turbulent Swirling Compressible Flow in Axisymmetric Ducts with Struts. NASA CR-2365, 1974.

TABLE I. - INLET COORDINATES

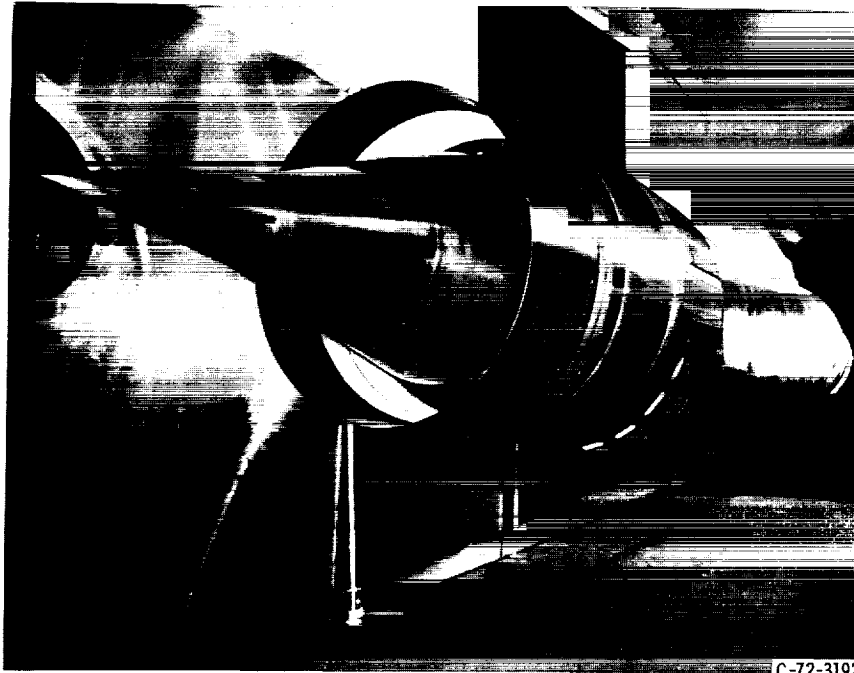
(a) Cowl				(b) Mach 2.5 centerbody				(c) Mach 2.0 centerbody			
x/R	r/R	x/R	r/R	x/R	r/R	x/R	r/R	x/R	r/R	x/R	r/R
2.0148	1.0000	4.0148	0.9745	0	0	3.8542	0.6777	0	0	3.8542	0.5541
2° Internal cowl angle		4.0683	.9746	12.5° Conical section		3.9077	.6709	12.5° Conical section		3.9077	.5470
2.2117	1.0069	4.1218	.9748	1.0001	0.2217	3.9612	.6638	1.0001	0.2217	3.9612	.5397
2.2455	1.0079	4.1754	.9749	18.5° Conical section		4.0148	.6554	14.5° Conical section		4.0148	.5323
2.2761	1.0084	4.2289	.9751	2.3749	0.6817	4.0683	.6466	2.3509	0.5711	4.0683	.5248
2.3058	1.0086	4.2824	.9753	2.4408	.7036	4.1218	.6363	2.4053	.5851	4.1218	.5174
2.3348	1.0086	4.3360	.9756	2.5068	.7251	4.1754	.6255	2.4597	.5991	4.1754	.5100
2.3631	1.0082	4.3895	.9759	2.5733	.7463	4.2289	.6137	2.5144	.6128	4.2289	.5026
2.3908	1.0075	4.4430	.9761	2.5831	.7494	4.2824	.6016	2.5695	.6264	4.2824	.4951
2.4180	1.0065	4.4965	.9763	Bleed slot		4.3360	.5893	2.6160	.6377	4.3360	.4877
2.4447	1.0053	4.5501	.9765	2.6883	0.7547	4.3895	.5768	Bleed slot		4.3895	.4803
2.4710	1.0038	4.6036	.9768	2.7283	.7526	4.4430	.5645	2.7222	0.6429	4.4430	.4728
2.4971	1.0021	4.6571	.9770	2.7836	.7497	4.4965	.5521	2.7836	.6397	4.4965	.4654
2.5381	0.9993	4.7107	.9771	2.8371	.7469	4.5501	.5397	2.8371	.6369	4.5501	.4580
2.5786	.9967	4.7642	.9774	2.8906	.7441	4.6036	.5273	2.8906	.6341	4.6036	.4505
2.6187	.9944	4.8177	.9776	2.9442	.7413	4.6571	.5149	2.9442	.6313	4.6571	.4431
2.6584	.9924	4.8713	.9779	2.9977	.7384	4.7107	.5025	2.9977	.6285	4.7107	.4357
2.6978	.9906	4.9242	.9781	3.0512	.7356	4.7642	.4902	3.0512	.6257	4.7642	.4282
2.7369	.9889	4.9783	.9783	3.1048	.7328	4.8177	.4778	3.1048	.6229	4.8177	.4208
2.7760	.9872	5.0319	.9785	3.1583	.7300	4.8713	.4654	3.1583	.6200	4.8713	.4134
2.7836	.9869	5.0854	.9787	3.2118	.7272	4.9248	.4530	3.2118	.6171	4.9248	.4060
2.8371	.9850	5.1389	.9790	3.2653	.7242	4.9783	.4406	3.2653	.6135	4.9783	.3985
2.8906	.9831	5.1924	.9792	3.3189	.7211	5.0319	.4282	3.3189	.6097	5.0319	.3911
2.9442	.9813	5.2460	.9794	3.3724	.7179	5.0854	.4159	3.3724	.6055	5.0854	.3837
2.9977	.9794	5.2995	.9796	3.4259	.7146	5.1389	.4035	3.4259	.6011	5.1389	.3762
3.0512	.9778	5.3530	.9798	3.4795	.7110	5.1924	.3911	3.4795	.5963	5.1924	.3688
3.1048	.9763	5.4066	.9800	3.5330	.7072	5.2460	.3787	3.5330	.5912	5.2460	.3614
3.1583	.9754	5.4601	.9802	3.5865	.7032	5.2995	.3661	3.5865	.5858	5.2995	.3539
3.2118	.9748	5.5136	.9805	3.6401	.6990	5.3530	.3538	3.6401	.5803	5.3530	.3461
3.2653	.9745	5.5672	.9807	3.6936	.6942	5.4066	.3413	3.6936	.5741	5.4066	.3386
3.3189	.9743	5.6207	.9808	3.7471	.6892	5.4601	.3354	3.7471	.5677	5.4601	.3354
3.3612	.9743	5.6742	.9809	3.8007	.6836	5.5136	.3354	3.8007	.5610	5.5136	.3354
3.4148	.9743	5.7277	.9810								

TABLE II. - STATIC-PRESSURE-TAP LOCATIONS

(a) Cowl (b) Mach 2.5 centerbody (c) Mach 2.0 centerbody

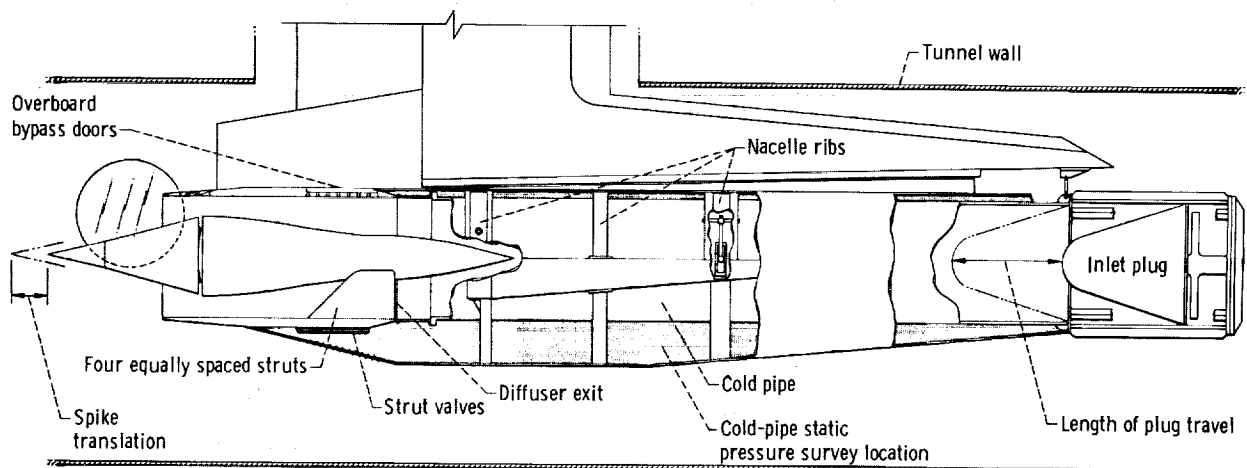
x/R		x/R		x/R	
2.088	3.158	0.910	^a 3.105	0.910	3.051
2.195	^a 3.212	.964	3.158	.964	^a 3.105
2.302	^a 3.319	1.028	^a 3.212	1.028	3.158
2.409	^a 3.426	1.081	^a 3.319	1.081	^a 3.212
2.462	3.533	1.820	^a 3.426	1.820	^a 3.319
2.516	3.640	2.034	3.533	2.034	^a 3.426
^a 2.569	3.747	2.248	3.640	2.248	3.533
2.623	3.854	2.409	3.747	2.409	3.640
^a 2.677	3.961	2.462	3.854	2.516	3.747
2.730	4.175	2.569	3.961	2.569	3.854
^a 2.784	4.389	^a 2.730	4.175	2.607	3.961
2.837	4.604	^a 2.784	4.389	^a 2.730	4.175
^a 2.891	4.818	2.837	4.604	2.757	4.389
2.944	5.139	^a 2.891	4.818	^a 2.784	4.604
^a 2.998	5.468	2.944	5.139	2.837	4.818
3.051	5.607	^a 2.998	5.468	^a 2.891	5.139
^a 3.105		^a 3.051	5.607	2.944	5.468
				^a 2.998	5.607

^aPressure taps located at 0° top centerline and 180° from top centerline; all other taps are located at top centerline only.



C-72-3192

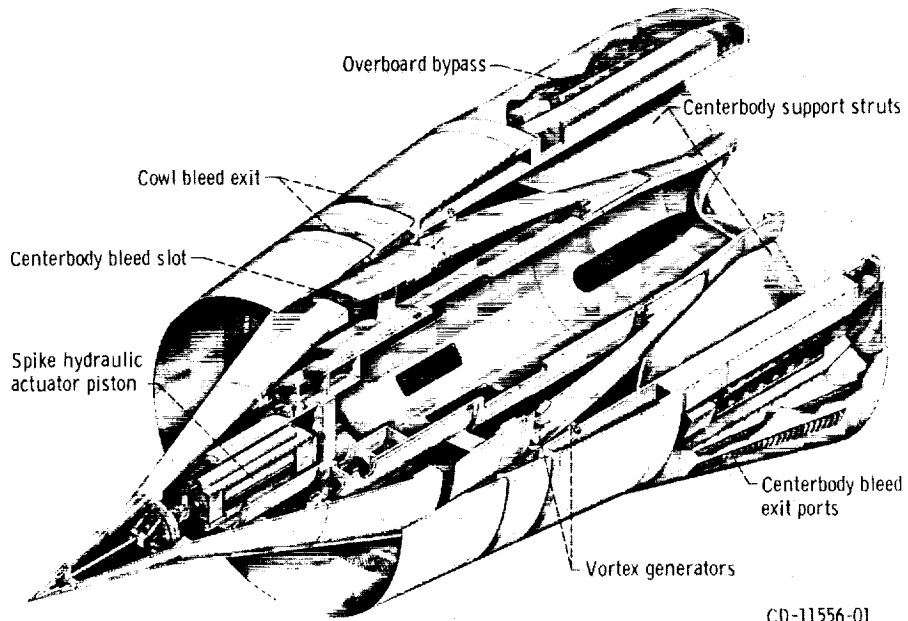
(a) Installation in 10- by 10-Foot Supersonic Wind Tunnel.



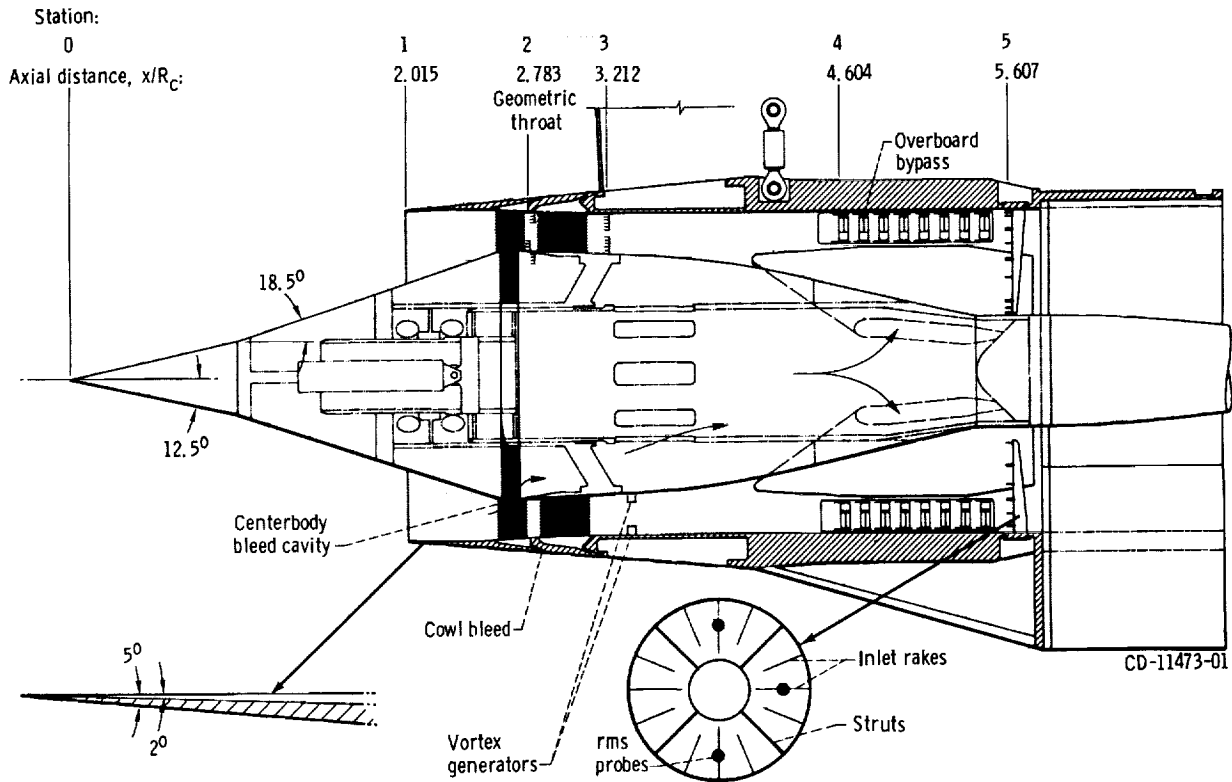
CD-11472-01

(b) Nacelle cutaway illustrating cold-pipe installation.

Figure 1. - Inlet model.



(a) Isometric view.



(b) Cross section and diffuser instrumentation.

Figure 2. - Details of inlet model.

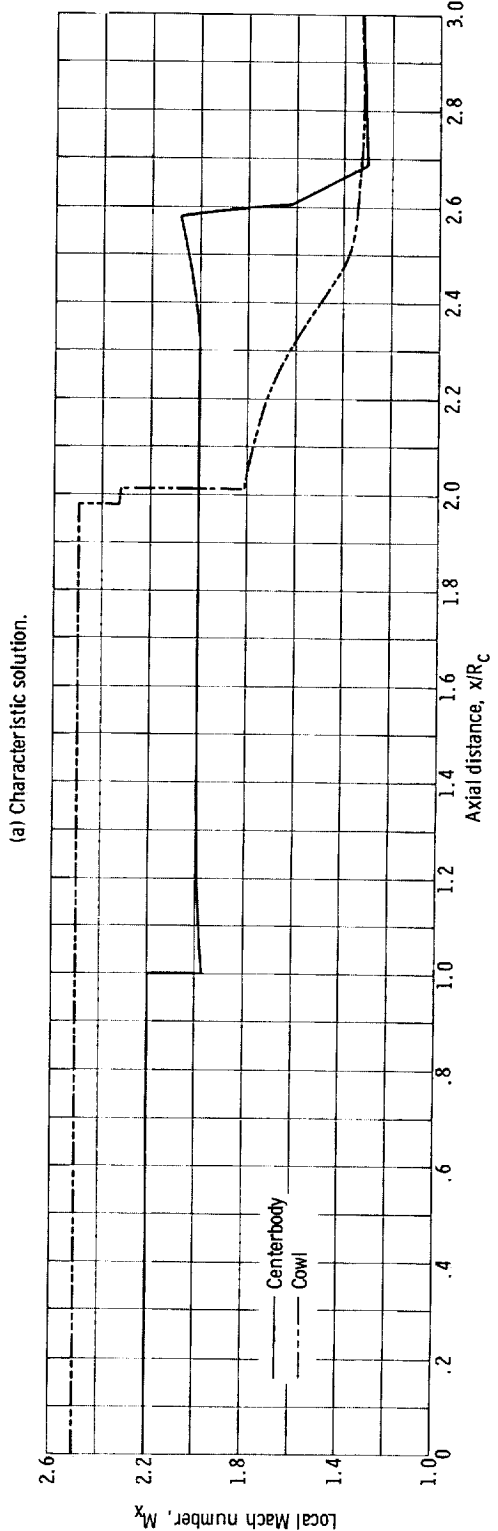
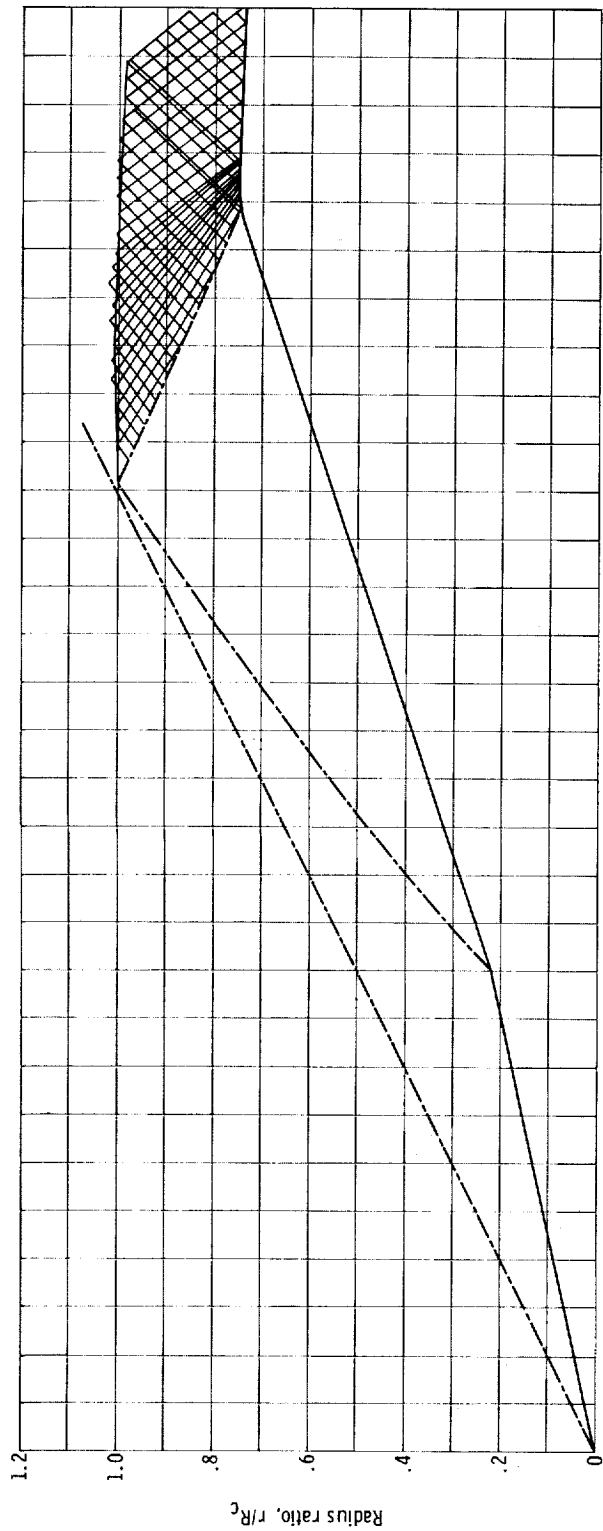
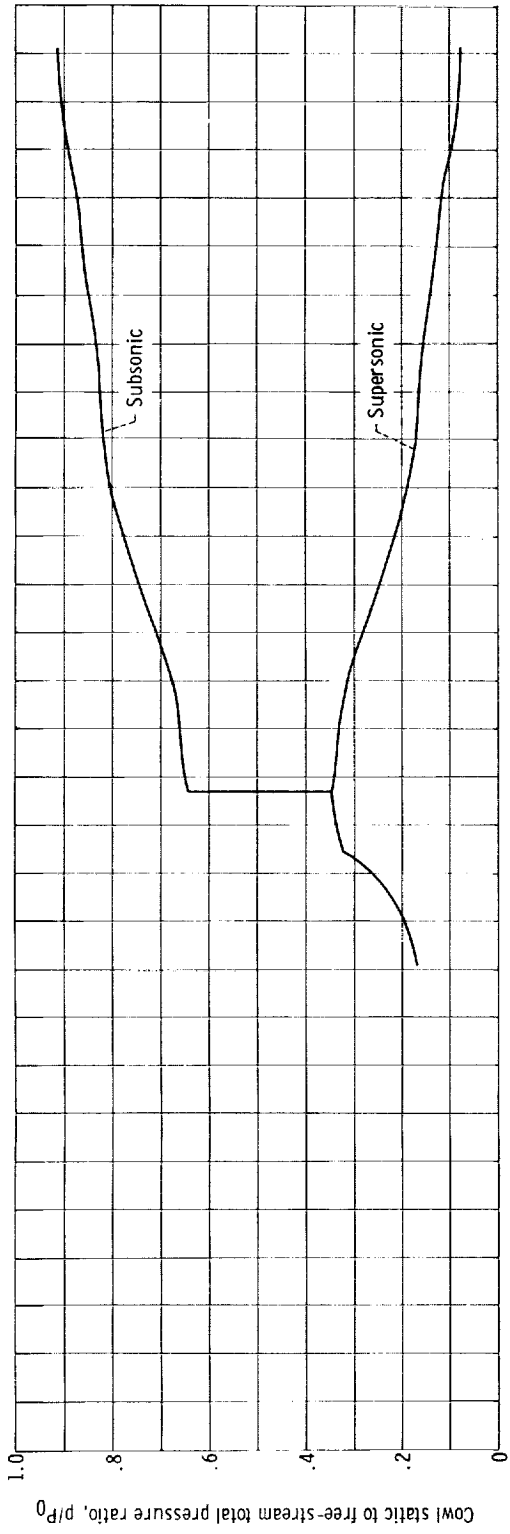
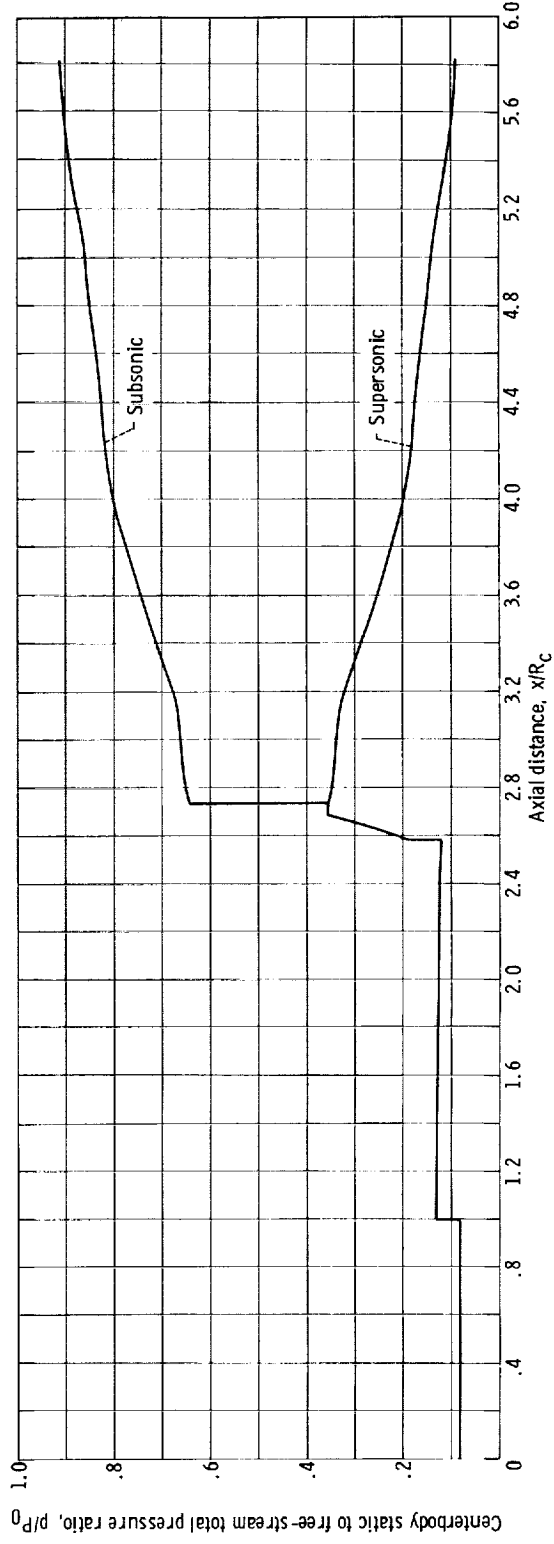


Figure 3 - Theoretical design of Mach 2.5 inlet.

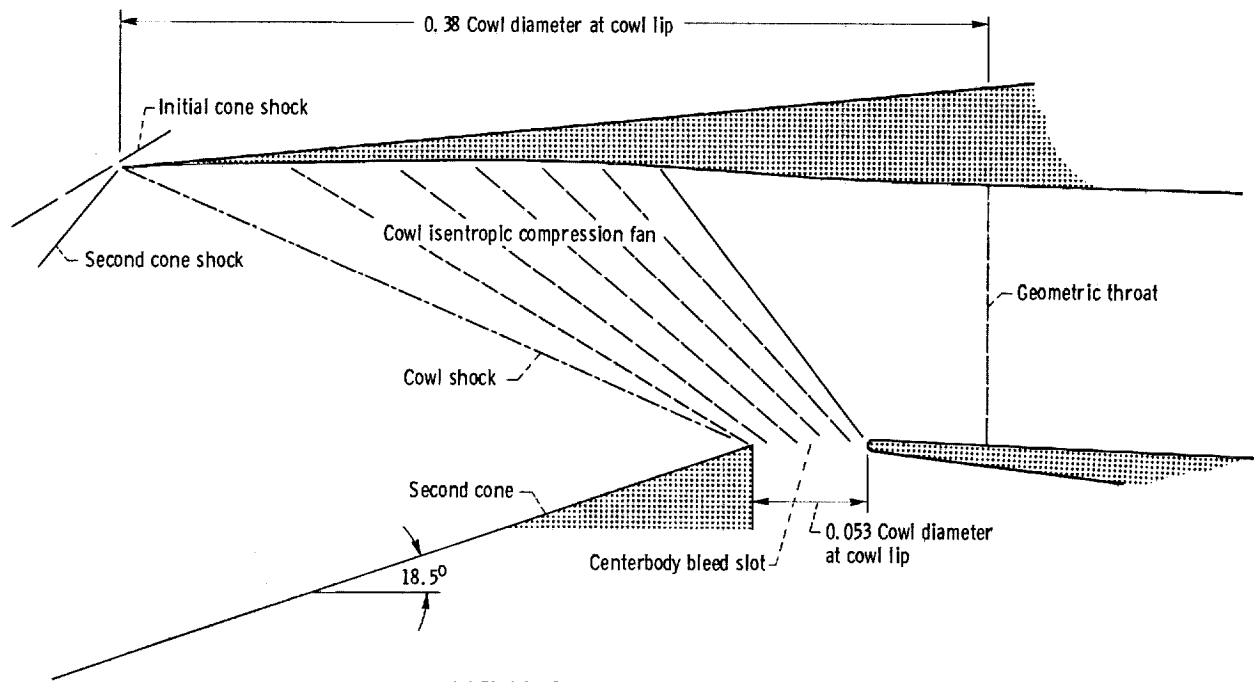


(c) Cowl pressure distribution.



(d) Centerbody pressure distribution.

Figure 3. - Continued.



(e) Sketch of supersonic diffuser details.

Figure 3. - Concluded.

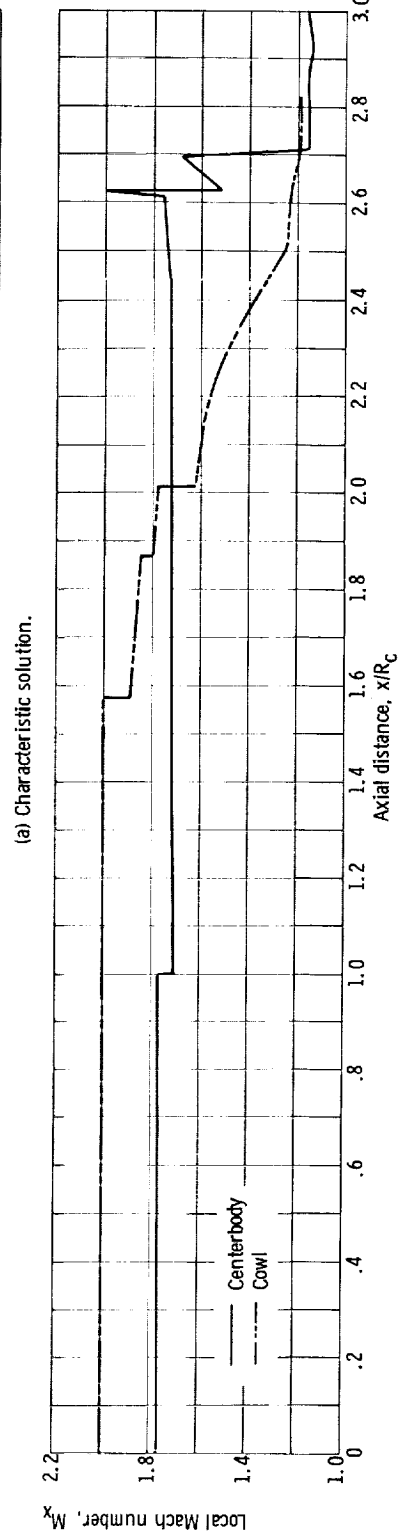
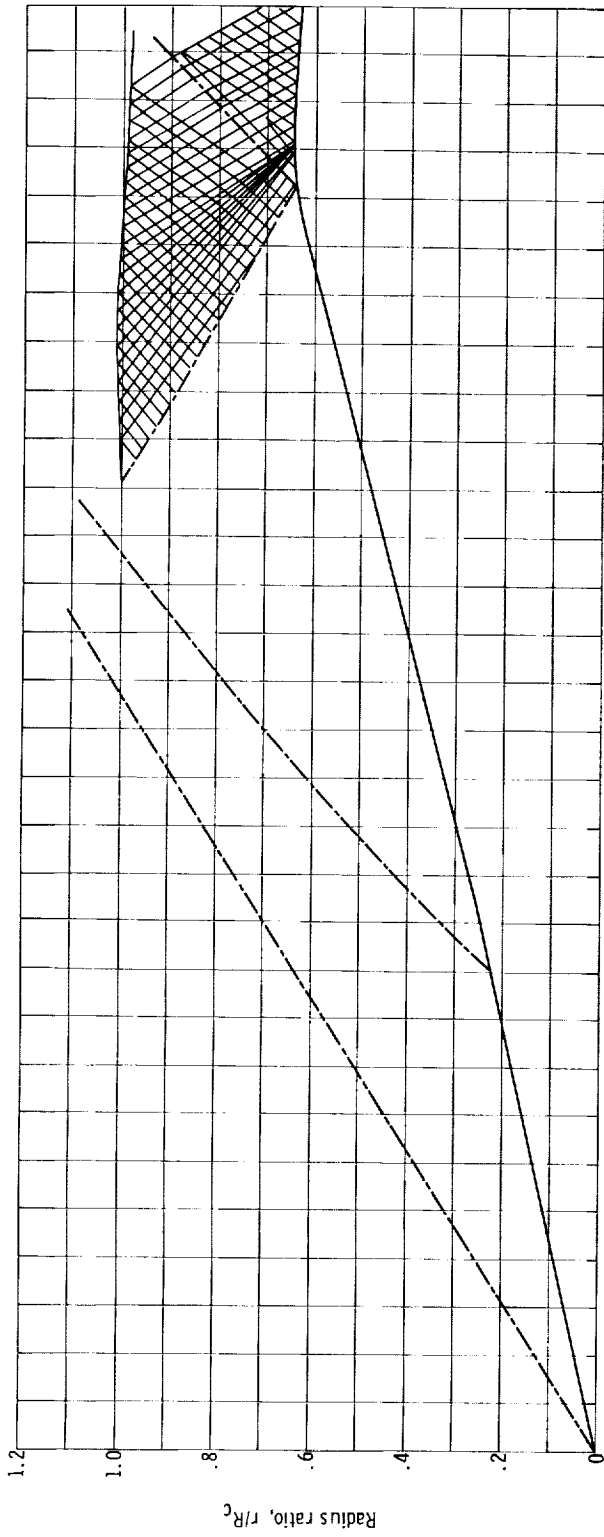


Figure 4. - Theoretical design of Mach 2.0 inlet.

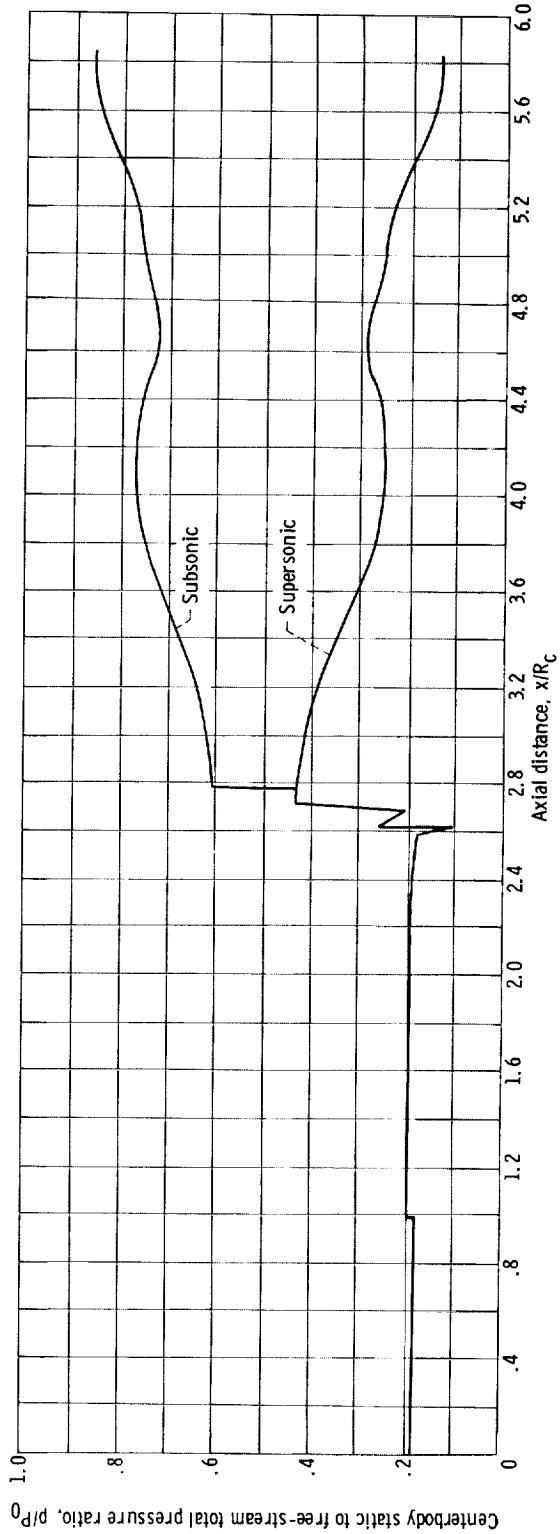
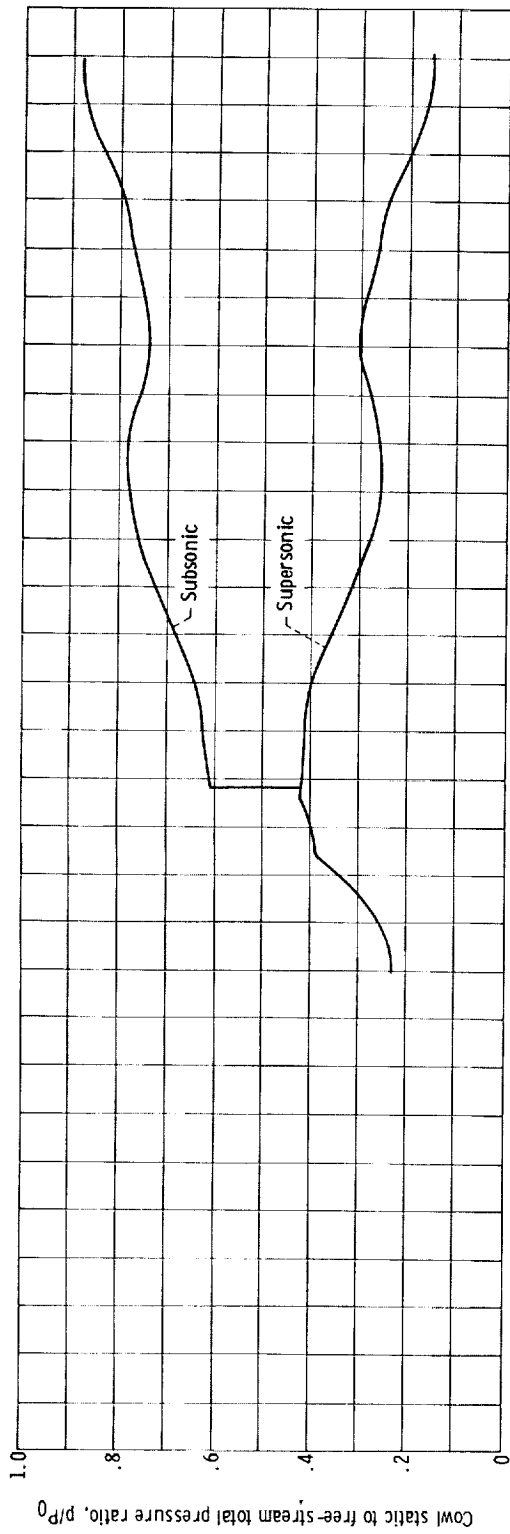
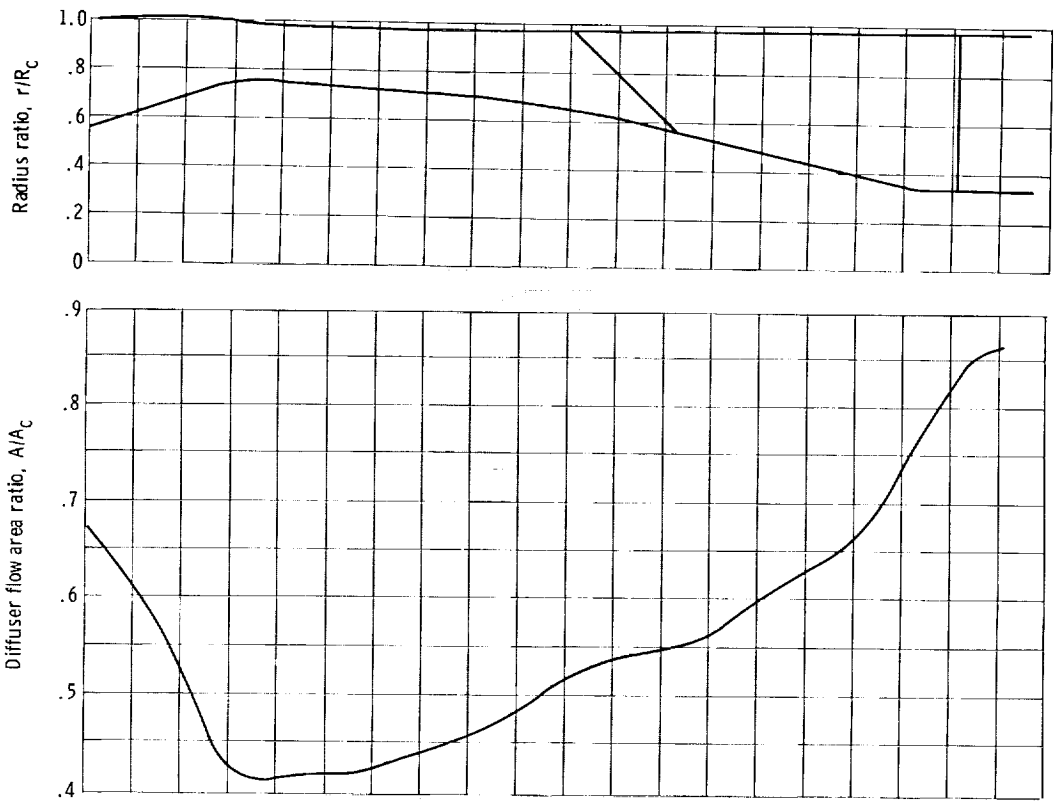
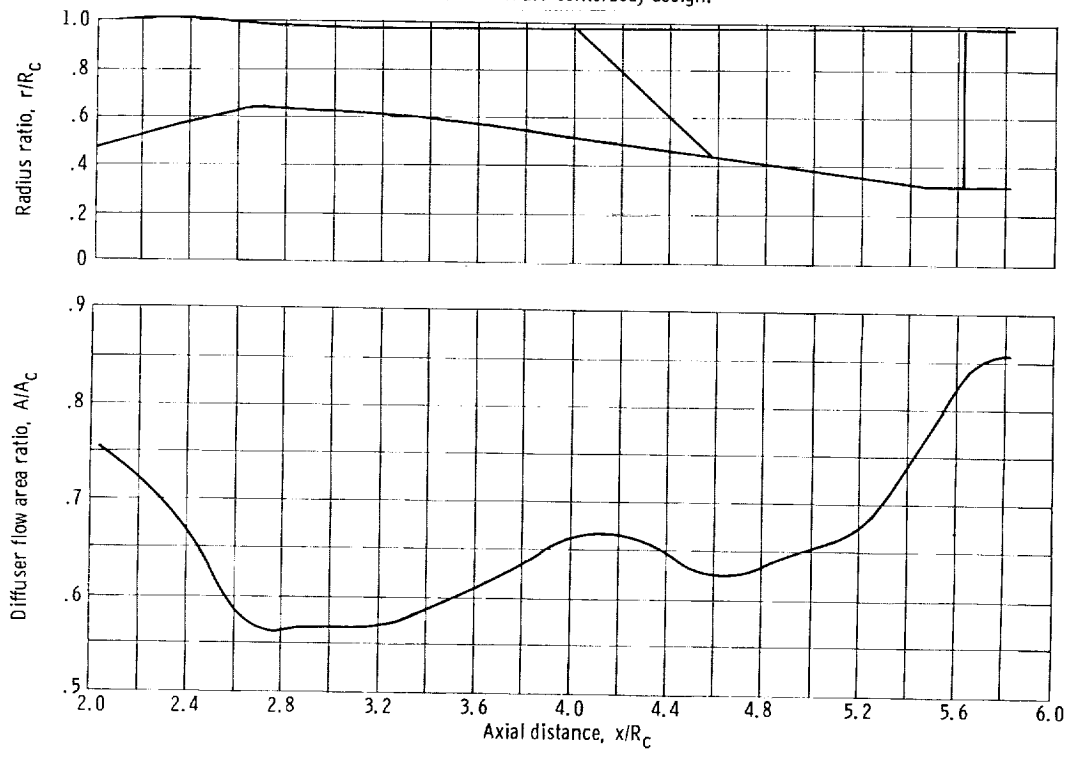


Figure 4. - Concluded.

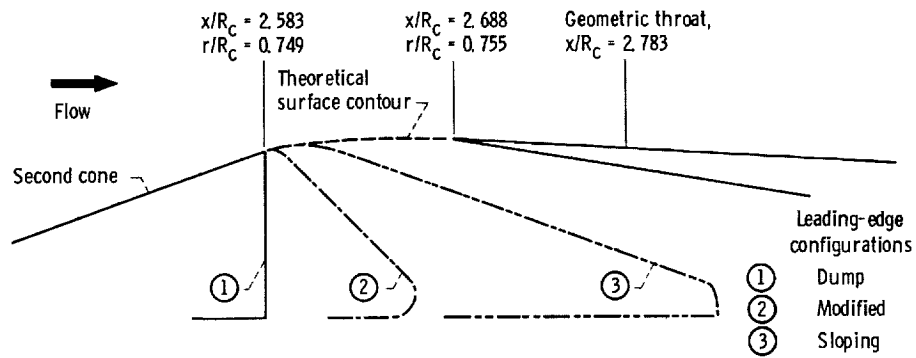


(a) Mach 2.5 centerbody design.

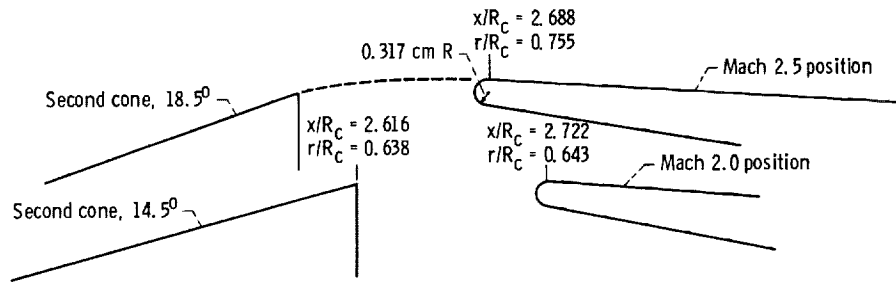


(b) Mach 2.0 centerbody design.

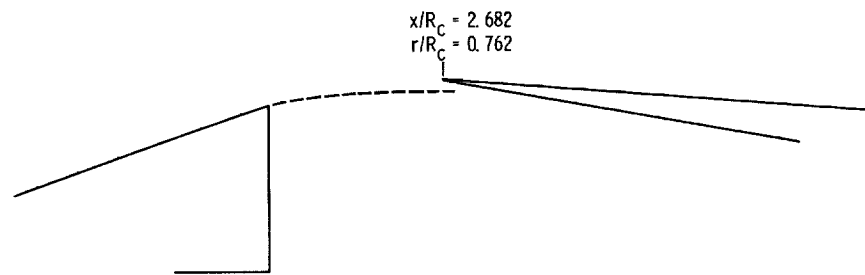
Figure 5. - Geometry of subsonic diffuser.



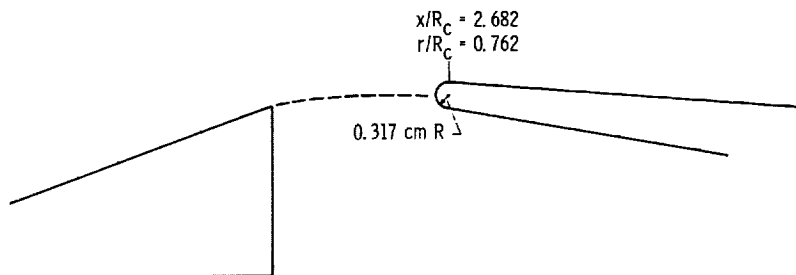
(a) Flush slot, sharp lip (configuration D).



(b) Flush slot, blunt lip (configuration A).



(c) Ram scoop, sharp lip (configuration B).



(d) Ram scoop, blunt lip (configuration C).

Figure 6. - Centerbody bleed configurations.

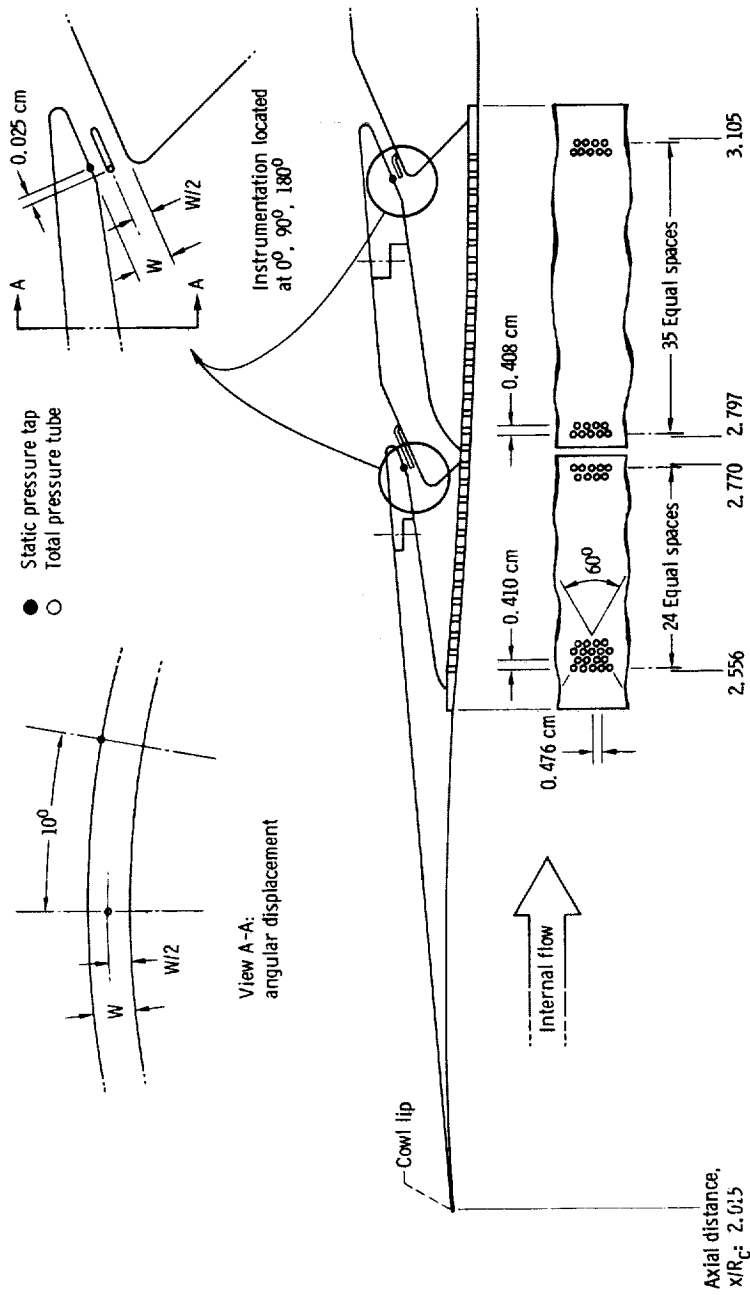
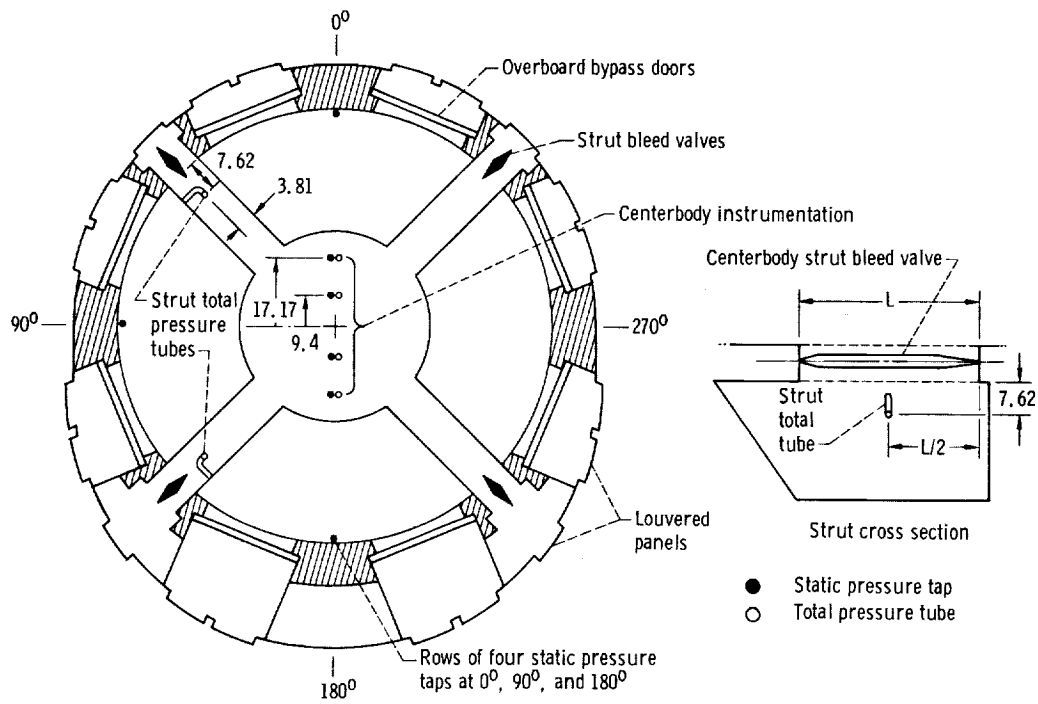
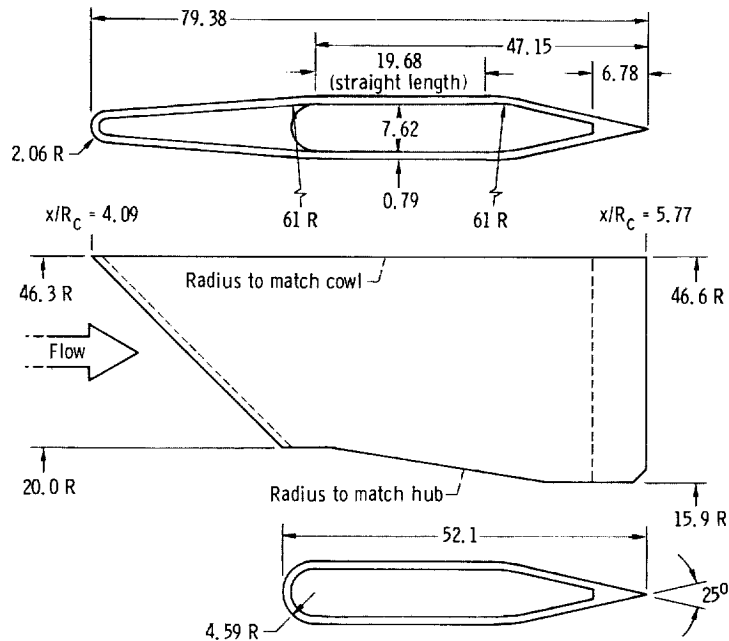


Figure 7. - Cowl bleed detail. Diameter of bleed holes, 0.3175 cm.

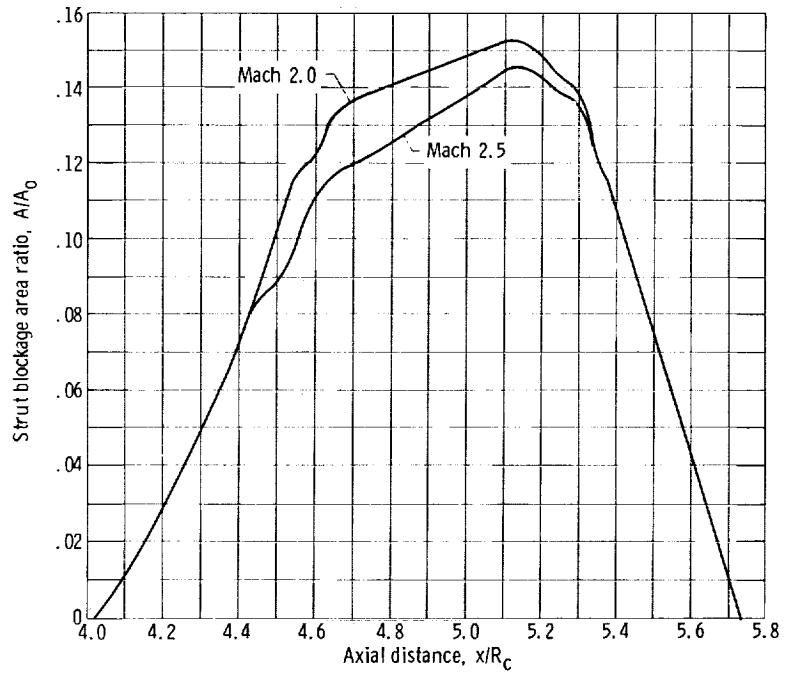


(a) Inlet cross section at struts.



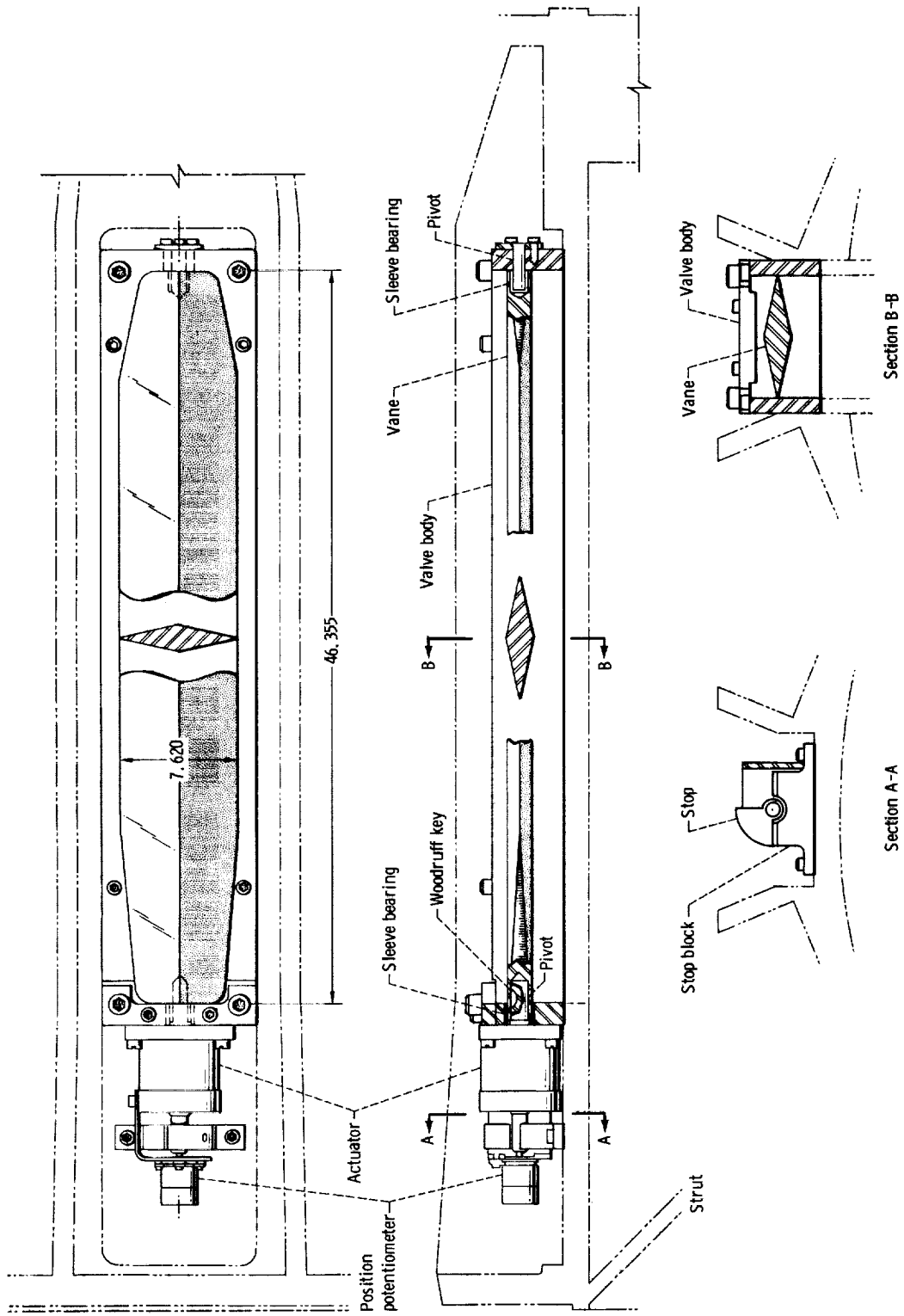
(b) Strut.

Figure 8. - Details of inlet support struts and strut valves. (All dimensions are in cm.)



(c) Blockage area of struts.

Figure 8. - Continued.



(d) Centerbody bleed strut valve.

Figure 8. - Concluded.

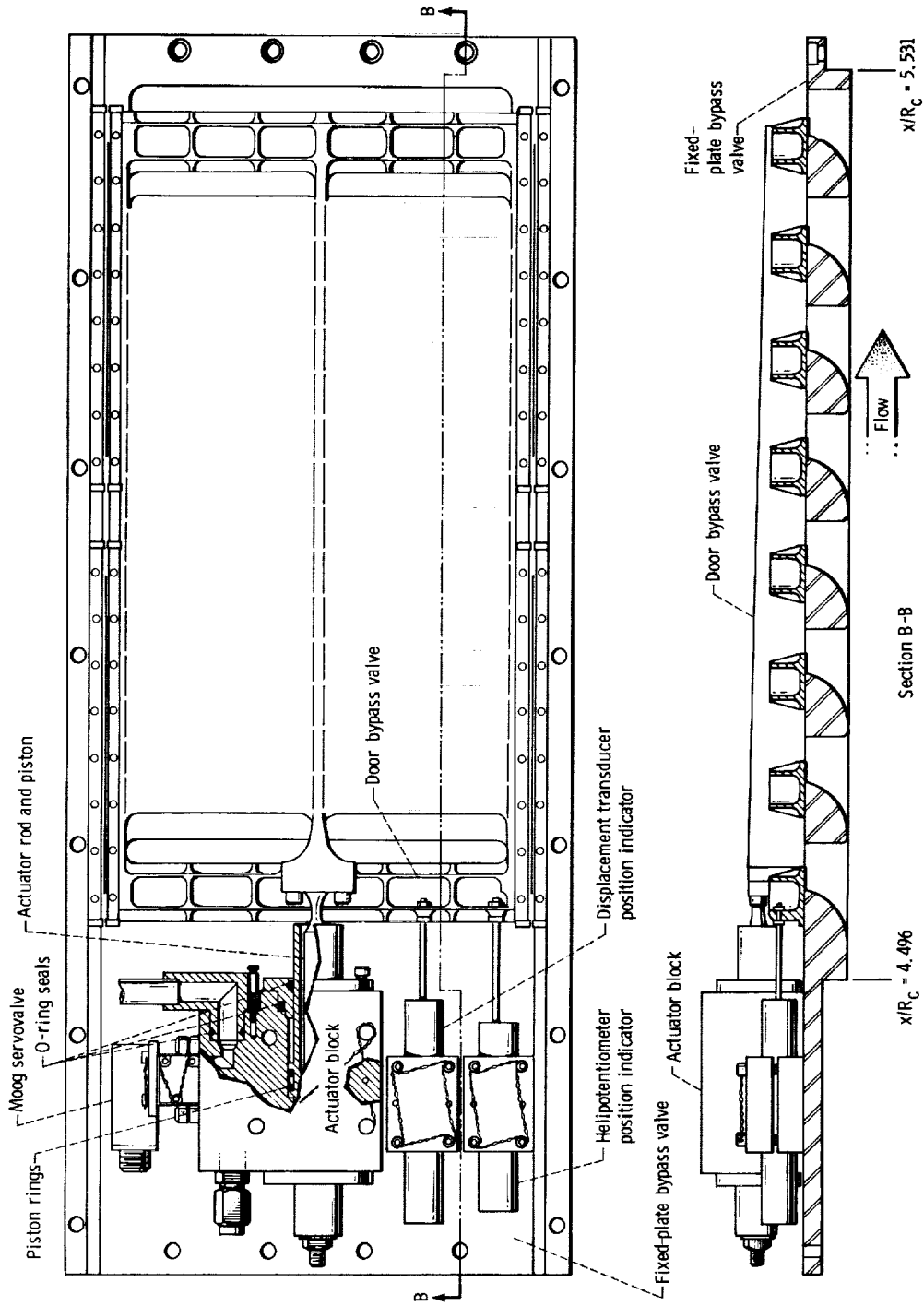
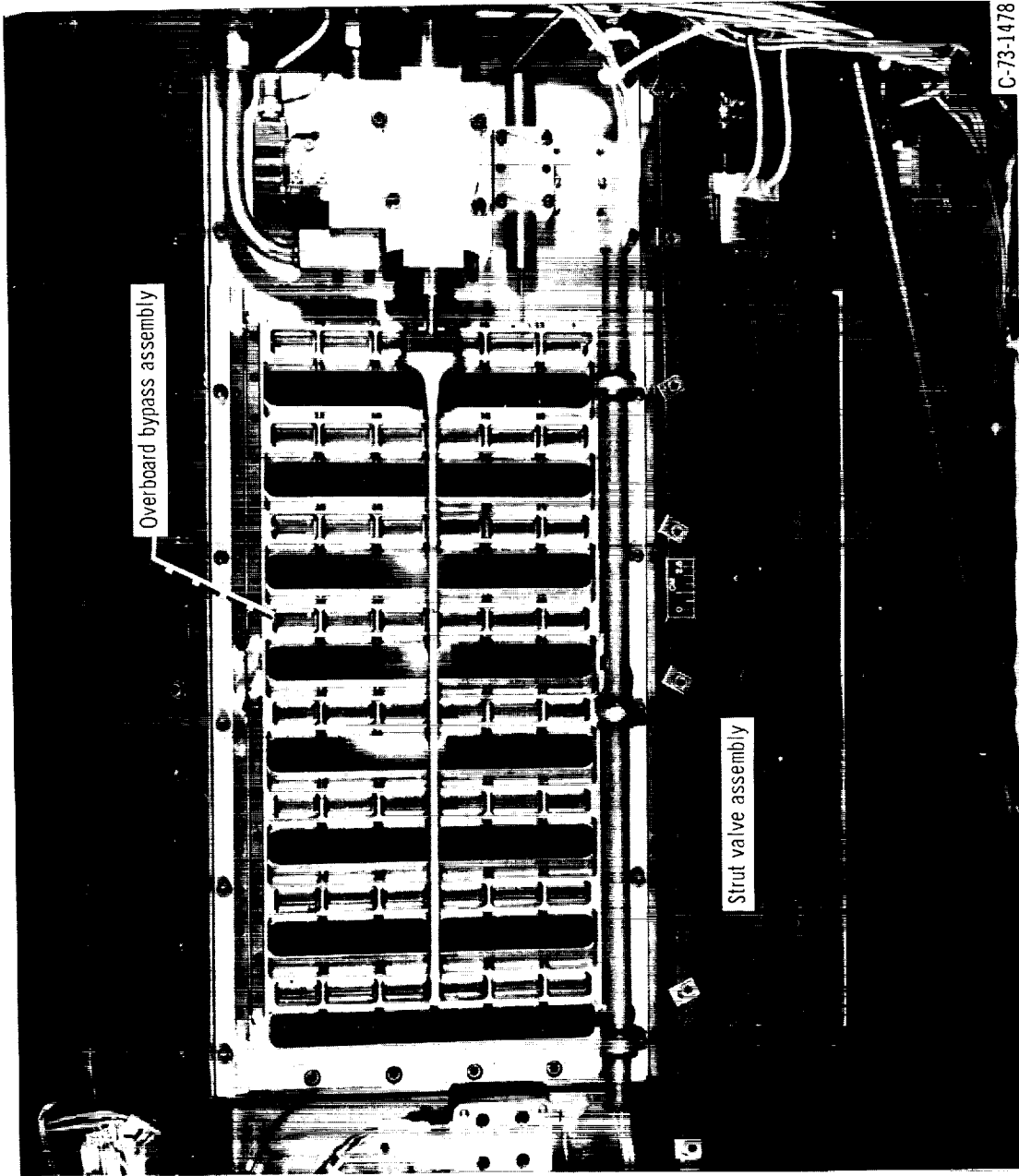


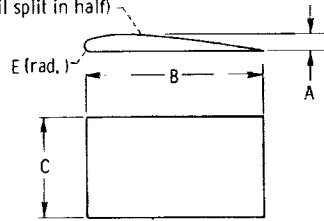
Figure 9. - Details of overboard bypass door.



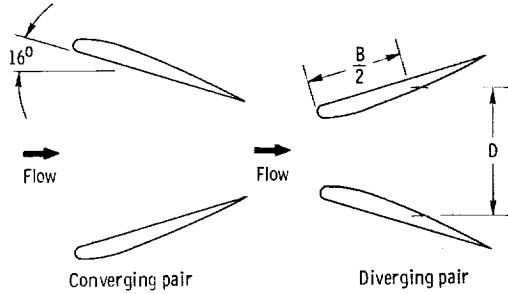
(b) Strut and overboard bypass valves installed.

Figure 9. - Concluded.

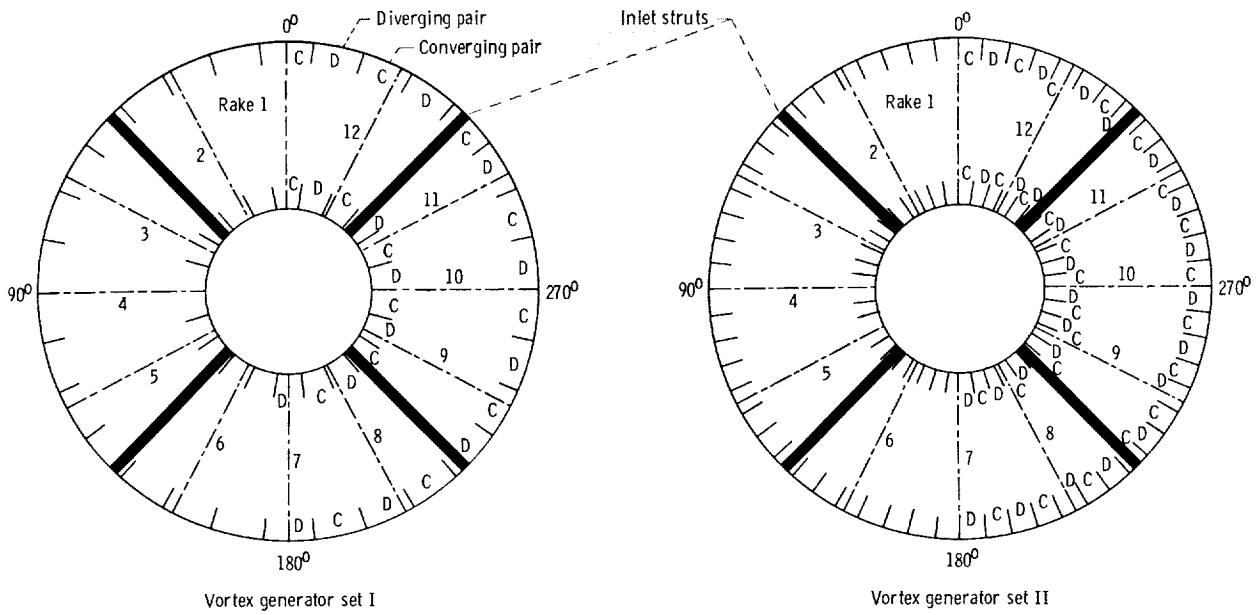
Upper surface coordinates from
NACA-0012 airfoil data
(airfoil split in half)



Set	Location	Dimension, cm				
		A	B	C	D	E
I	Cowl	0.305	5.044	2.54	9.682	0.051
	Centerbody	.305	5.044	2.54	9.723	.051
II	Cowl	0.229	3.048	1.52	4.841	0.030
	Centerbody	.305	4.064	2.03	4.862	.041

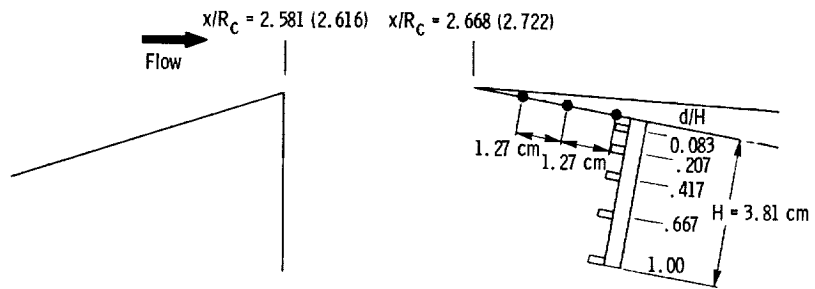


(a) Vortex generator detail.

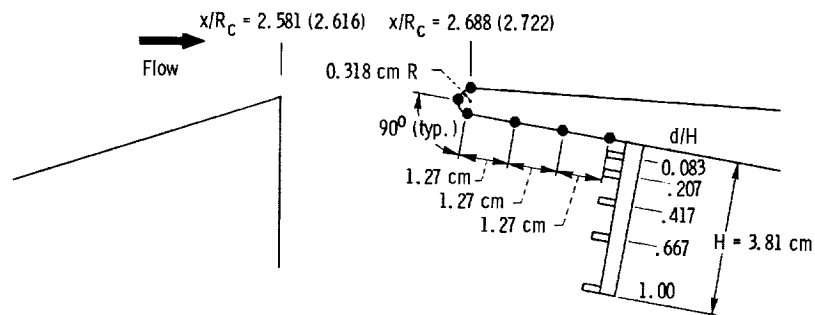


(b) Circumferential location, looking downstream.

Figure 10. - Vortex generator design.

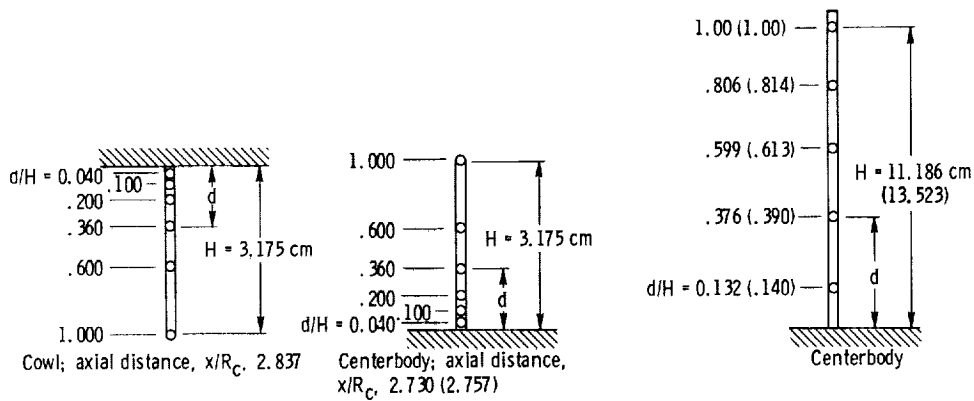


(a) Sharp lip - flush slot and ram scoop configurations.



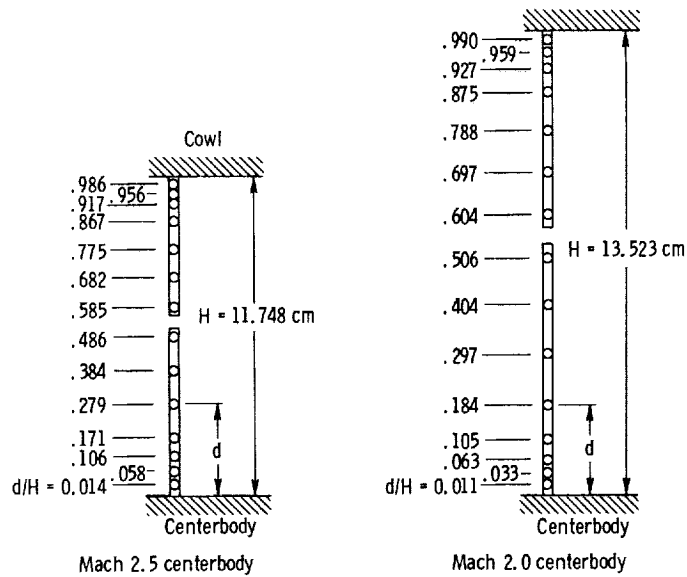
(b) Blunt lip - flush slot and ram scoop configurations.

Figure 11. - Centerbody bleed slot instrumentation. Static-pressure-tap location, 0° ; circumferential rake position, $\varphi, 10^\circ$. (Mach 2.0 centerbody coordinates are given in parentheses.)



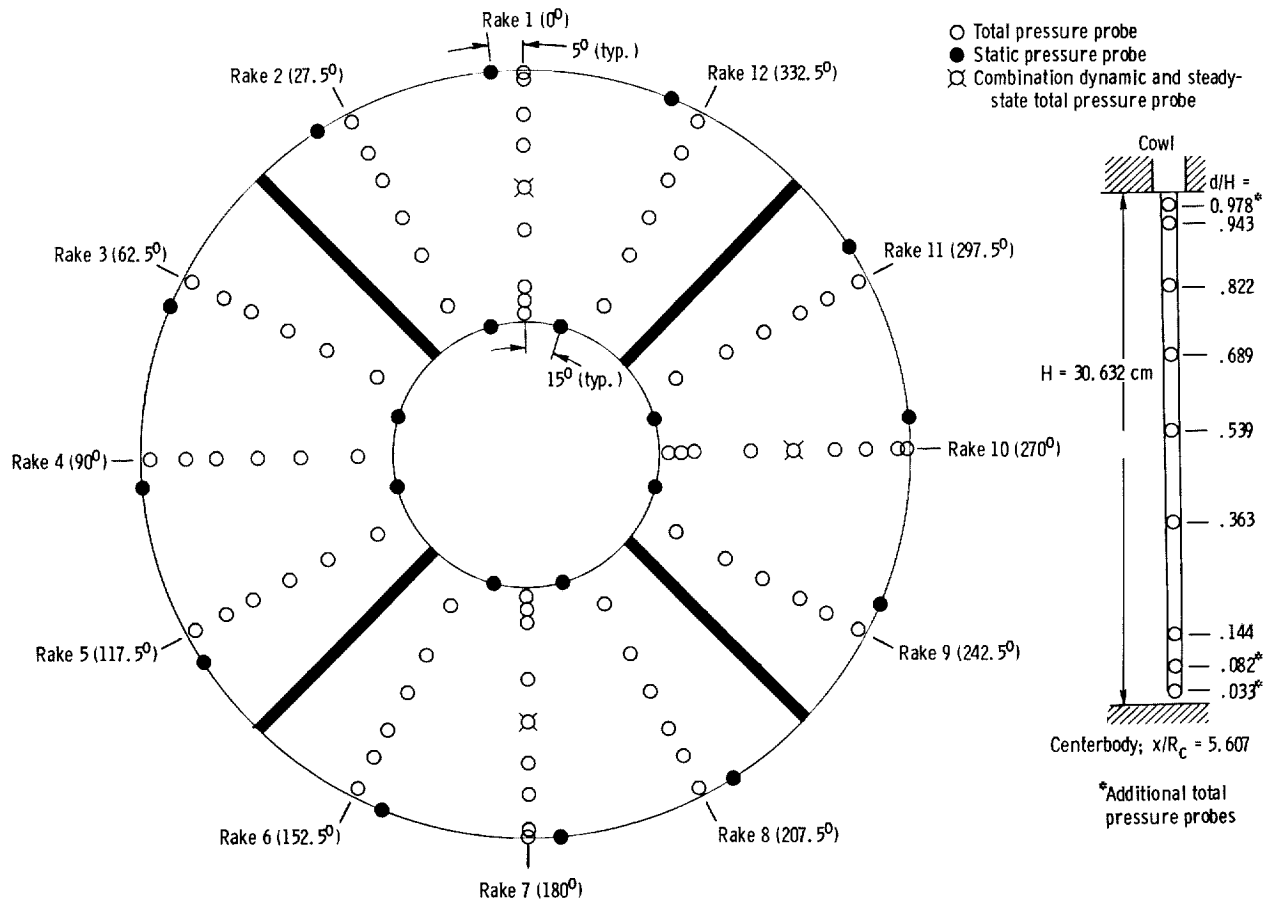
(a) Cowl and centerbody throat boundary layer total pressure rakes. Circumferential position, φ 10° . (Coordinate for Mach 2.0 centerbody is given in parentheses.)

(b) Mid-diffuser total pressure rake. Circumferential position, φ 0° ; axial distance, x/R_C , 4.604 (Dimensions for Mach 2.0 centerbody are given in parentheses.)



(c) Throat exit total pressure rakes. Circumferential position, φ 350° ; axial distance, x/R_C , 3.212.

Figure 12. - Inlet pressure instrumentation.



(d) Diffuser exit steady-state pressure instrumentation, at station 2 (looking downstream).

Figure 12. - Concluded.

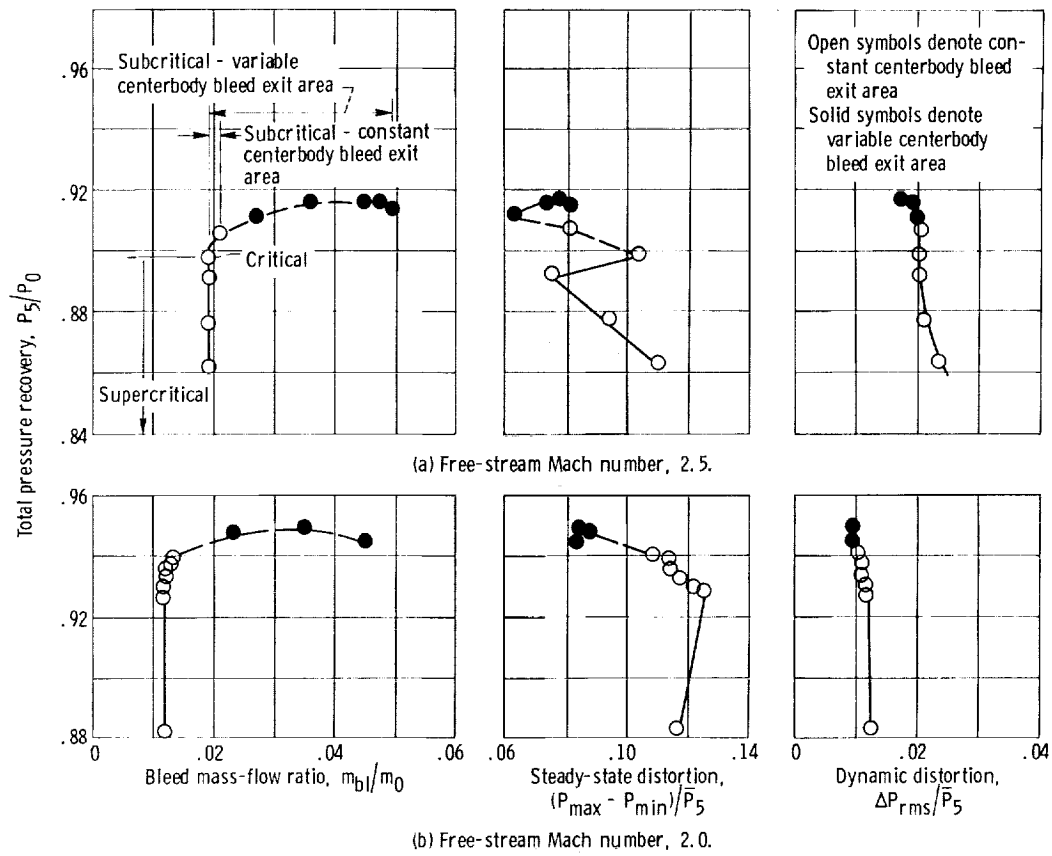


Figure 13. - Inlet performance with sealed bypass. Angle of attack, 0° ; cowl-lip-position parameter, $\theta_L = 26.4^\circ$.

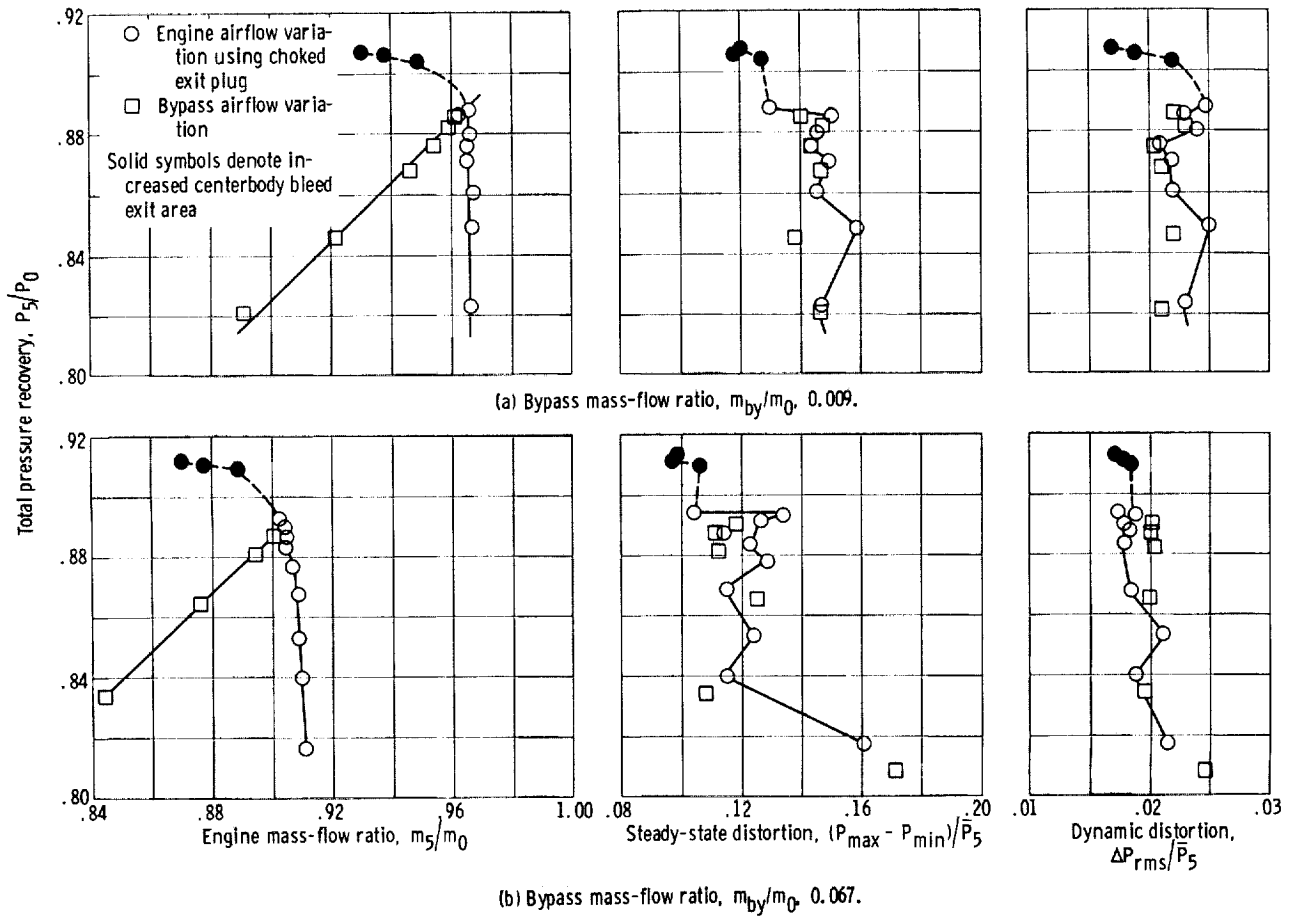


Figure 14. - Inlet performance with bypass flow at critical shock position. Free-stream Mach number, 2.5; angle of attack, 0° ; cowl-lip position parameter, θ_L , 26.4° .

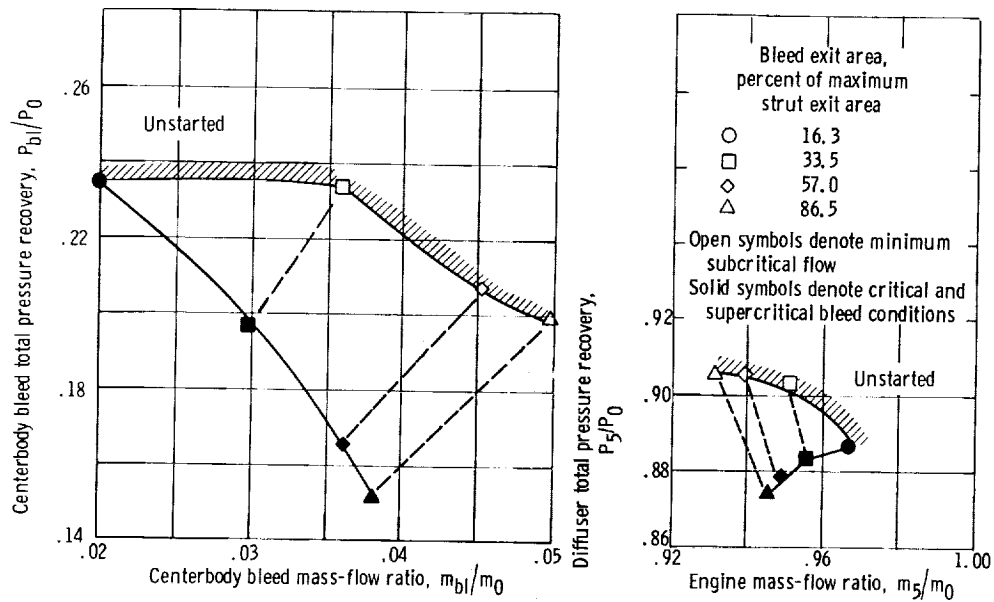


Figure 15. - Stability performance and bleed characteristics of centerbody bleed system. Free-stream Mach number, 2.5; angle of attack, 0° ; bypass mass-flow ratio, m_{by}/m_0 , 0.009.

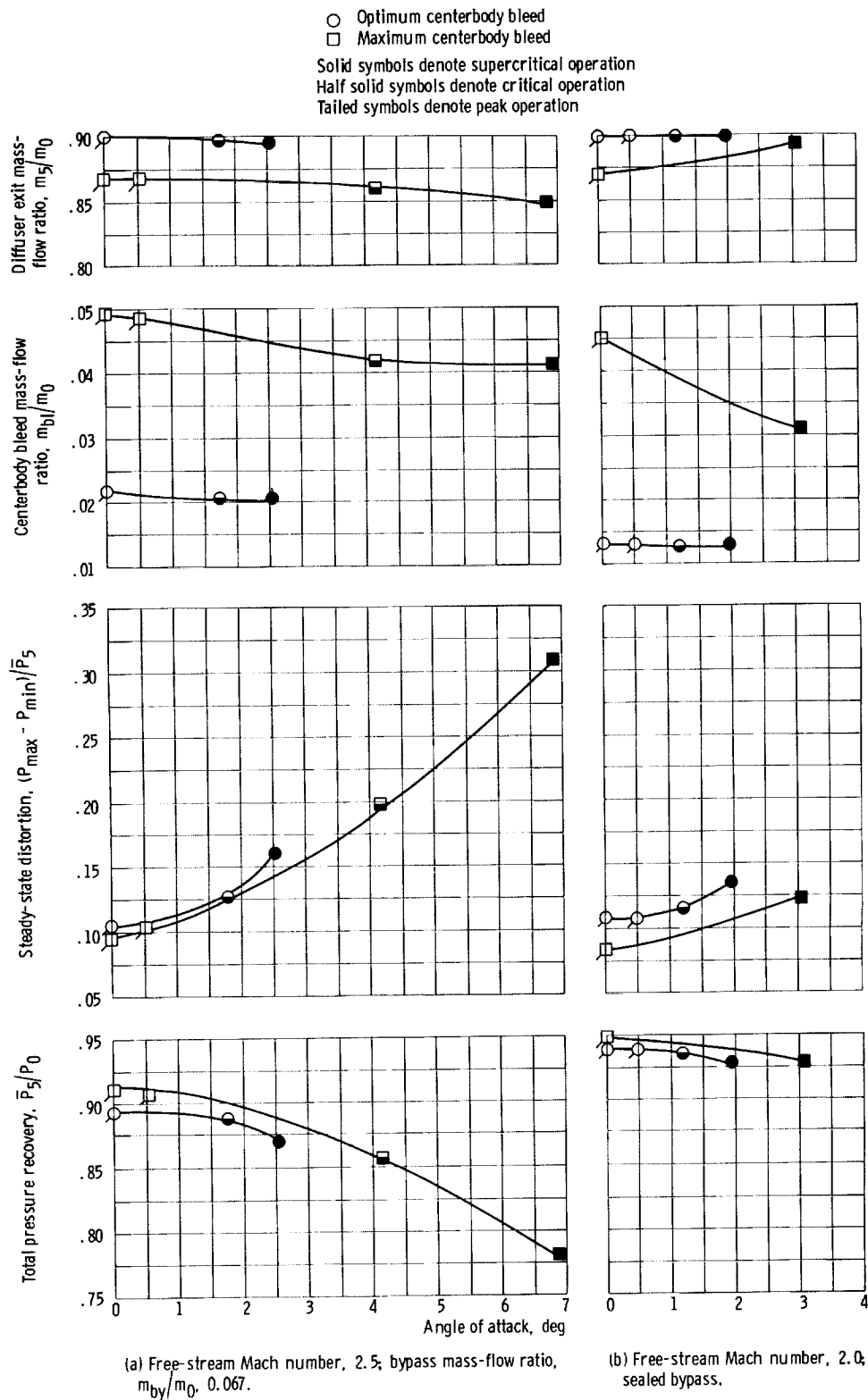
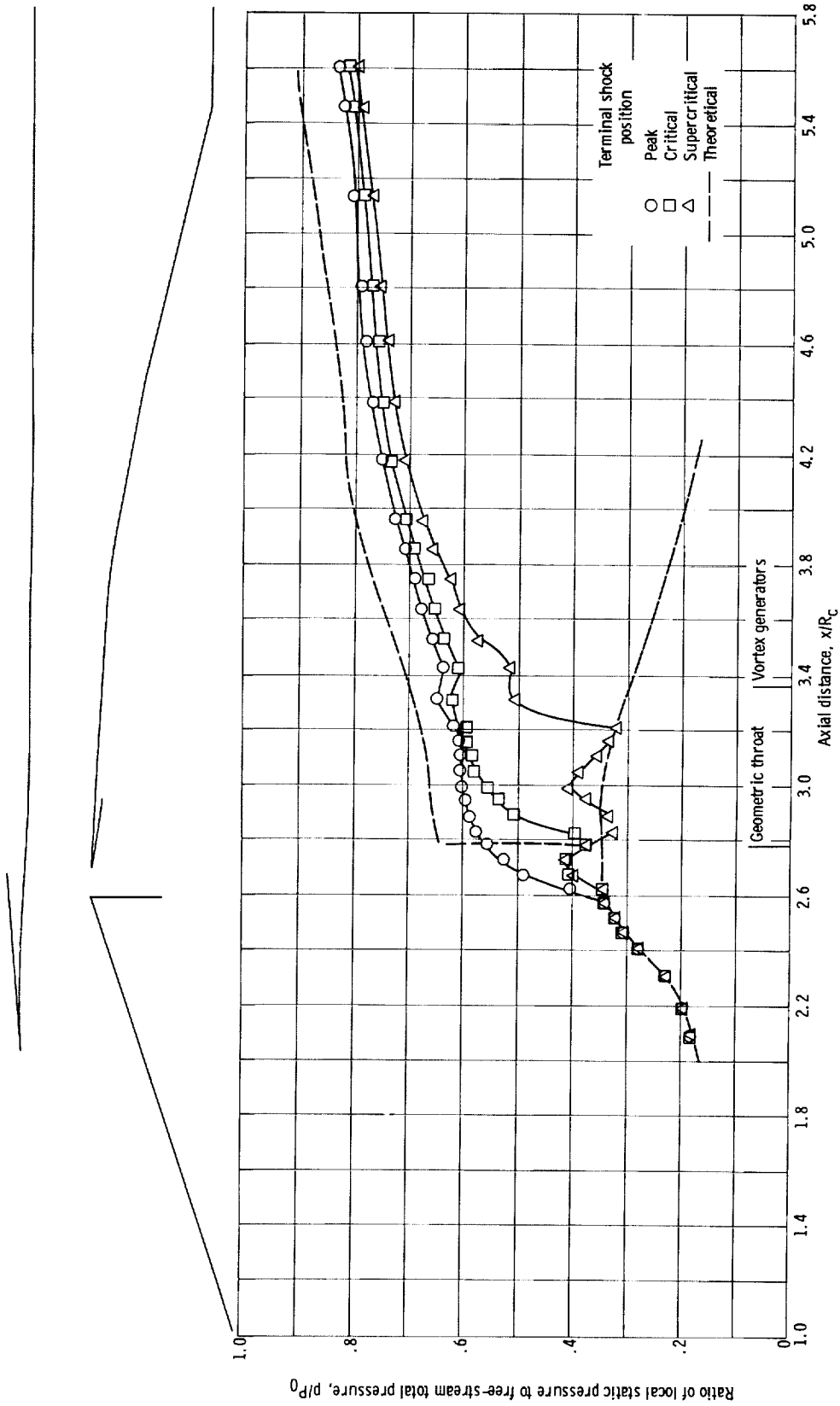
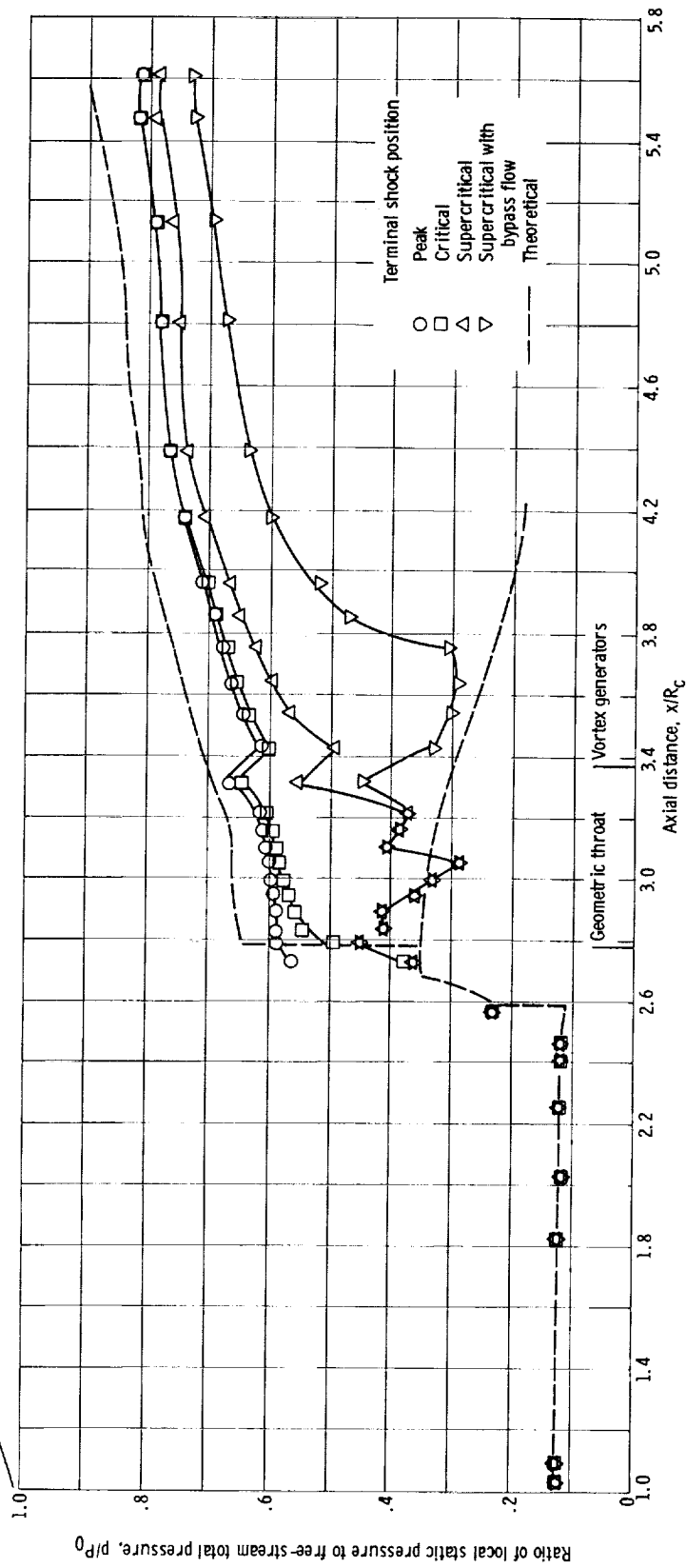


Figure 16. - Inlet angle of attack performance. Cowl-lip-position parameter, $\theta_L \approx 4^\circ$.



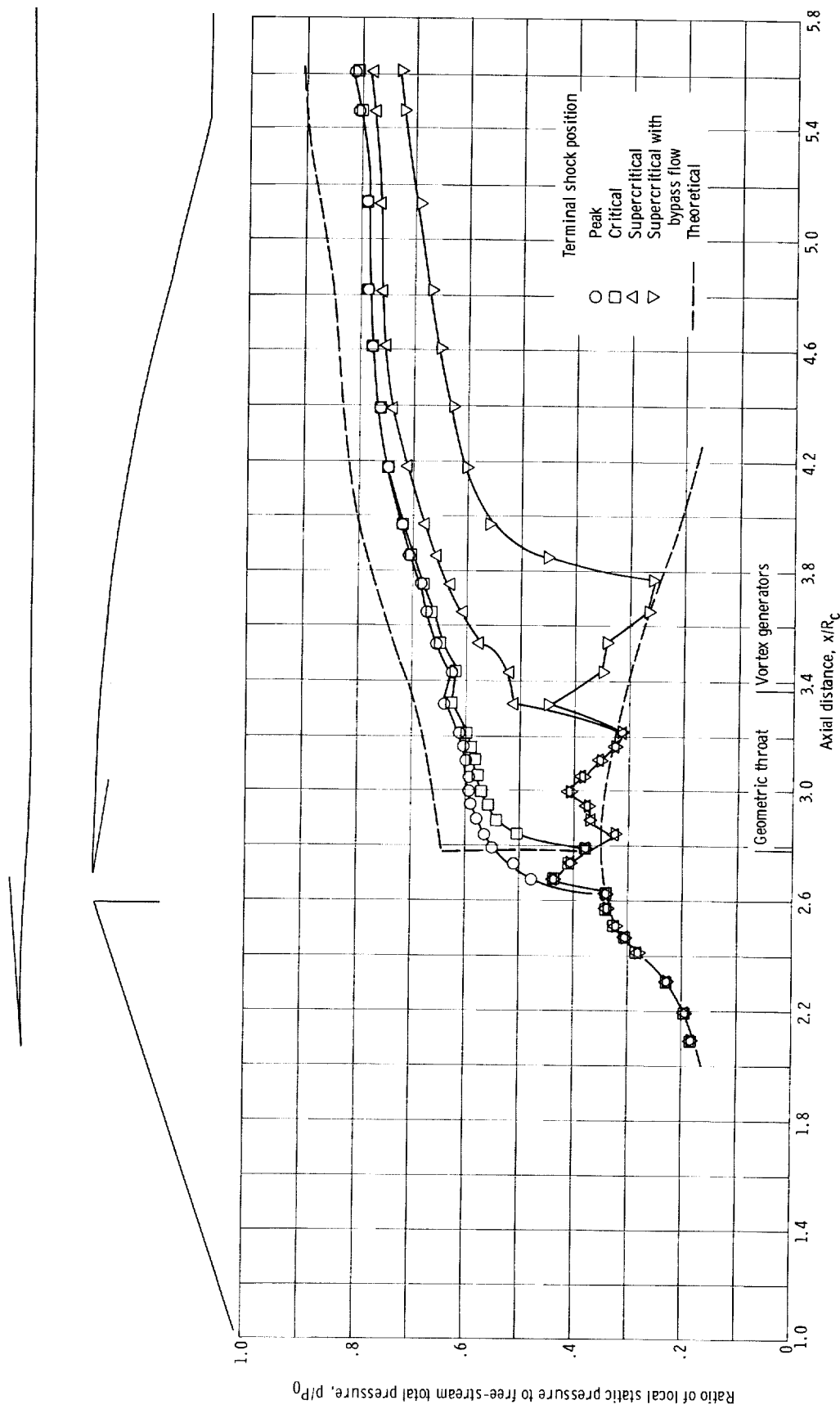
(b) Cowl, sealed bypass.

Figure 17. - Continued.



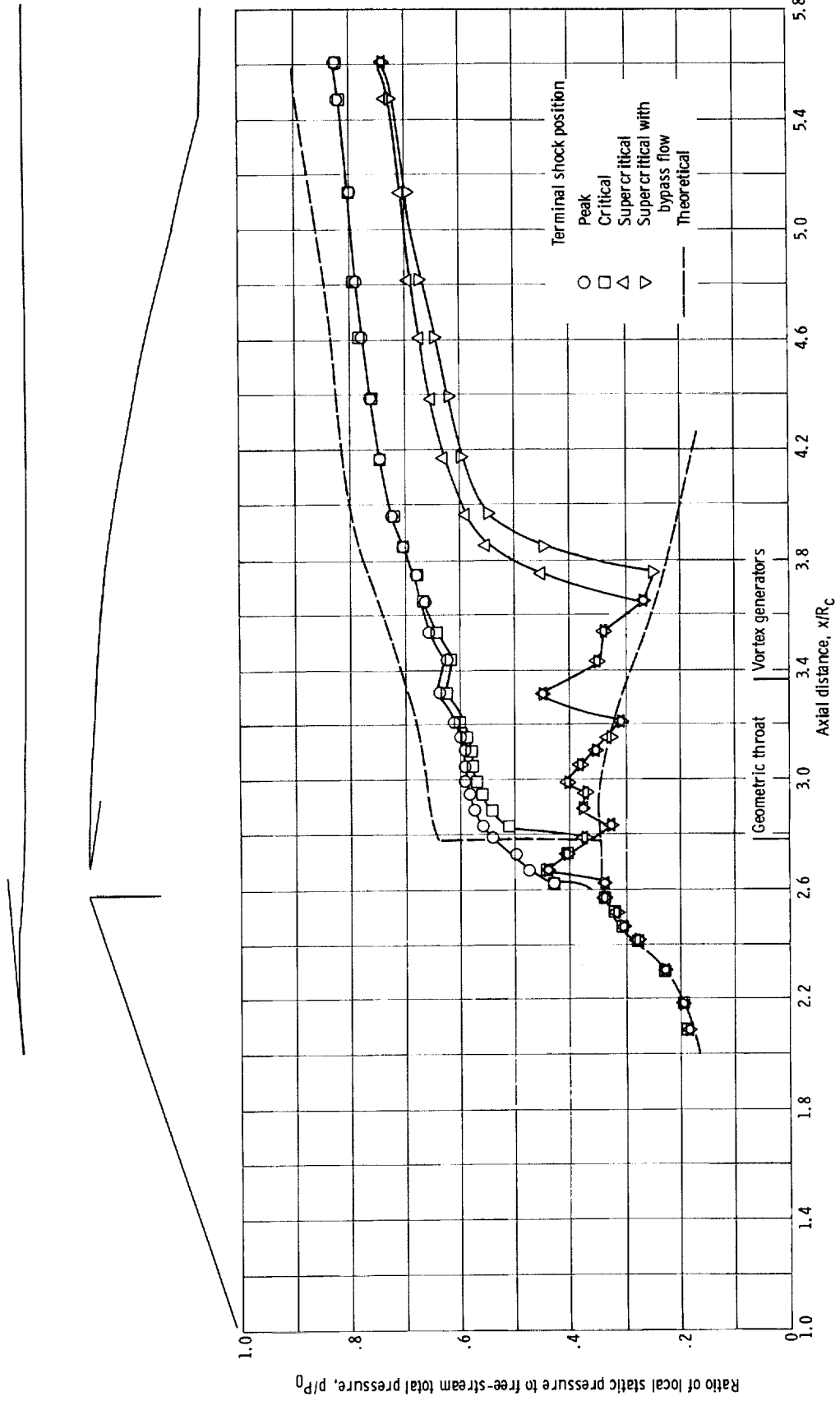
(c) Centerbody; bypass mass-flow ratio, m_{by}/m_0 , 0.009.

Figure 17. - Continued.

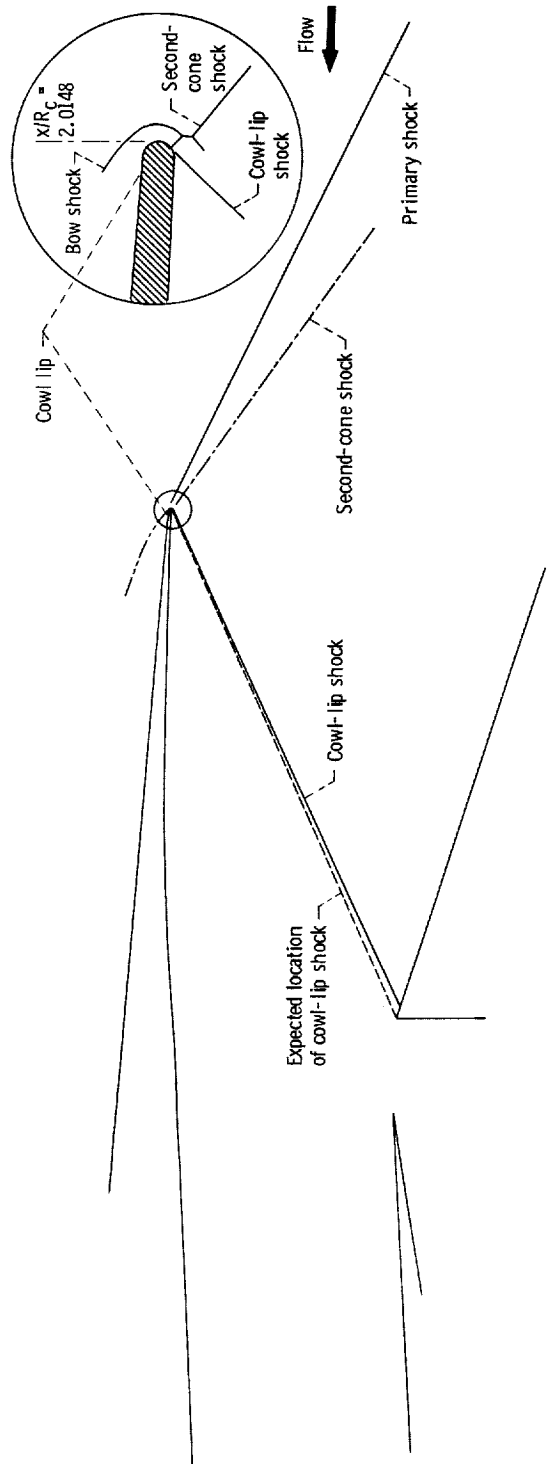


(d) Cowl; bypass mass-flow ratio, m_{by}/m_0 , 0.009.

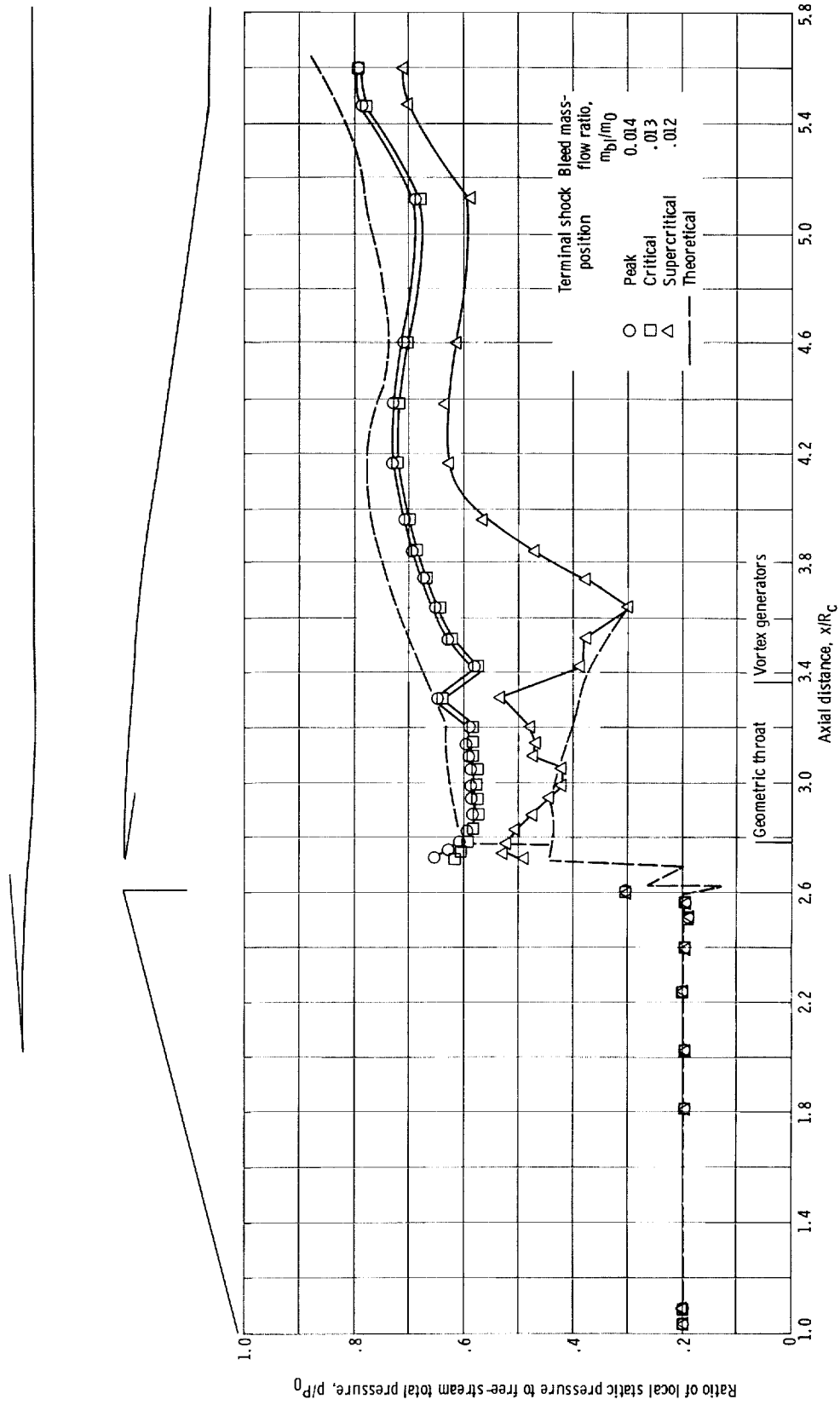
Figure 17. - Continued.



(f) Cowl; bypass mass-flow ratio, m_{by}/m_0 , 0.068.
Figure 17. - Continued.



(g) Cowl-lip shock structure.
Figure 17. - Concluded.



(a) Centerbody; sealed bypass.
 Figure 18. - Diffuser static pressure distributions at free-stream Mach number of 2.0. Angle of attack, θ^0 ; cowl-lip-position parameter, θ_L ; 26.4° .

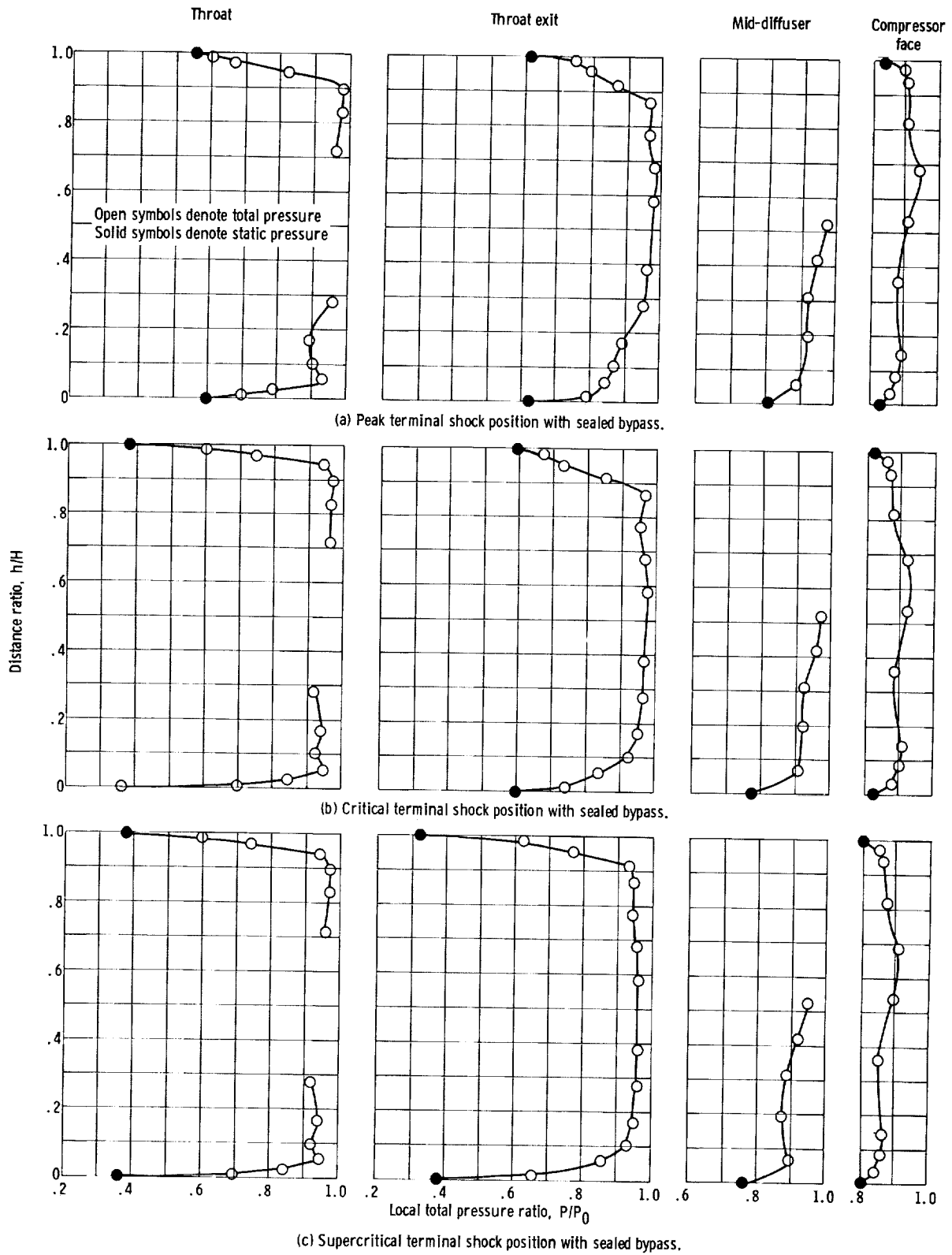


Figure 19. - Diffuser performance at Mach 2.5. Angle of attack, α^0 ; cowl-lip-position parameter, θ_2 26.4 0 ; bleed mass-flow ratio, m_{bl}/m_0 0.020.

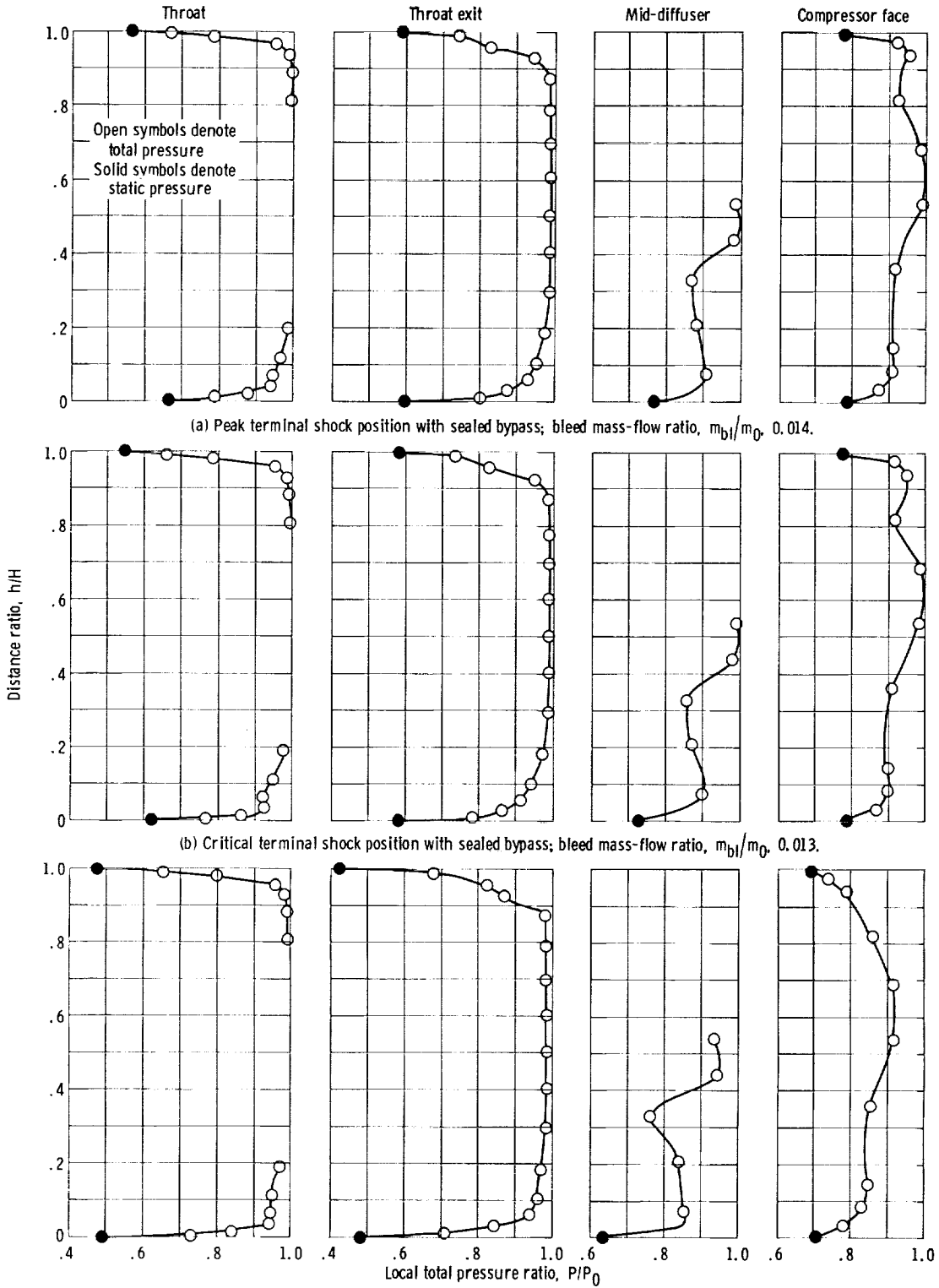


Figure 20. - Diffuser performance at Mach 2.0. Angle of attack, 0° ; cowli-lip-position parameter, θ_l , 26.4° .

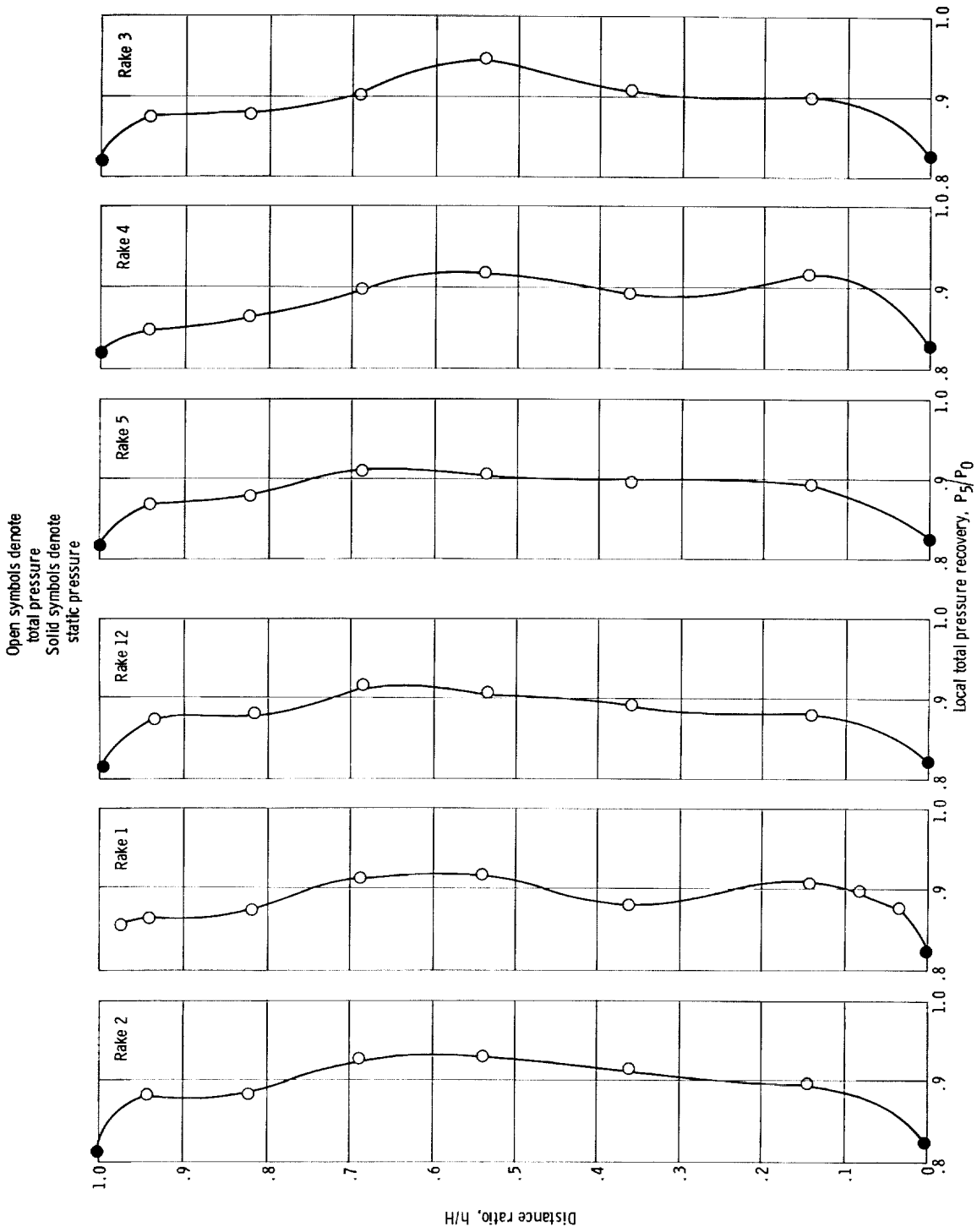
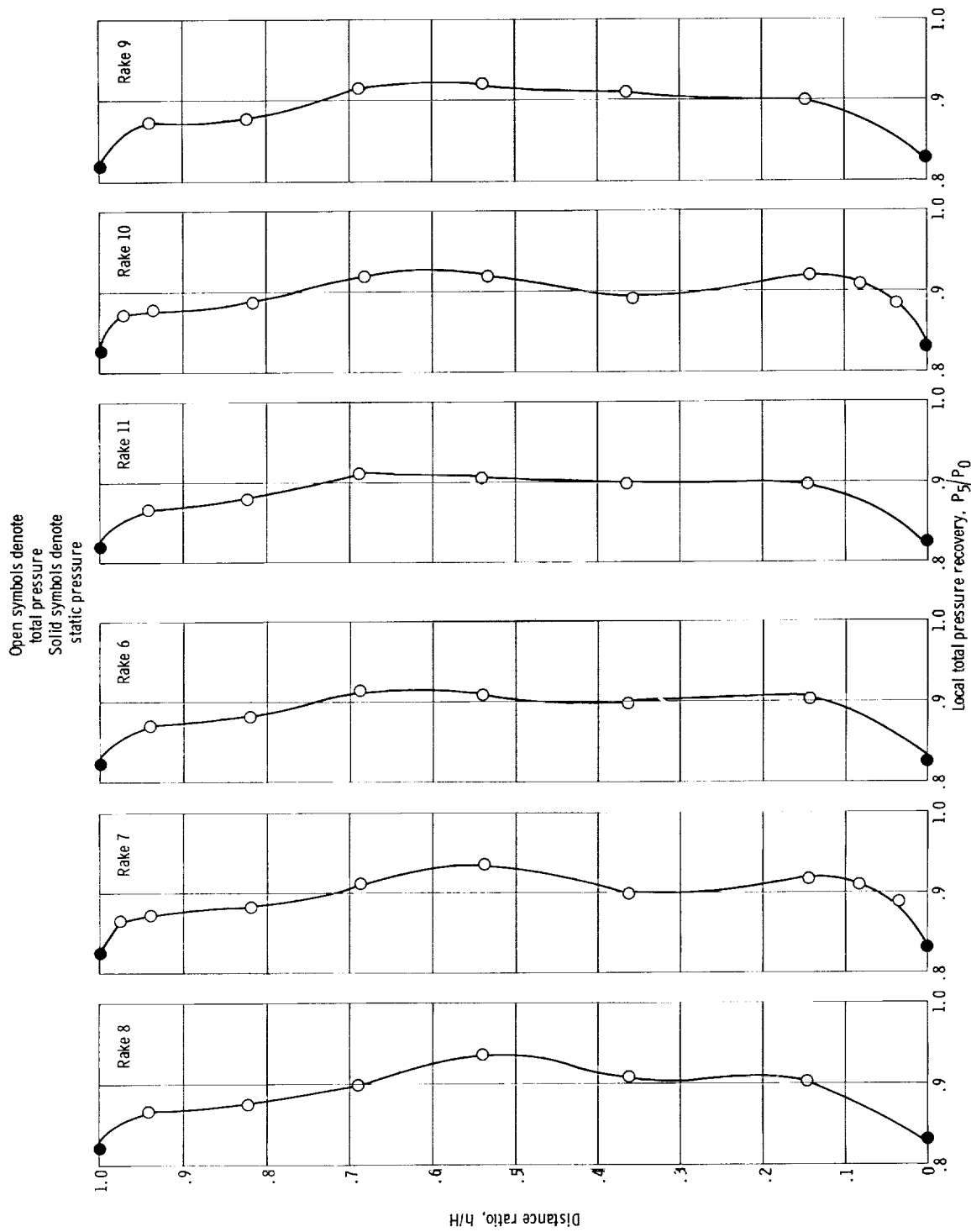


Figure 21. - Compressor face total pressure profiles for critical inlet operation and sealed bypass at free-stream Mach number of 2.5. Angle of attack, θ° ; cowl-lip position parameter, θ_t 26.4 $^{\circ}$; performance bleed, m_{bl}/m_0 0.019; average pressure recovery, P_5/P_0 0.898.

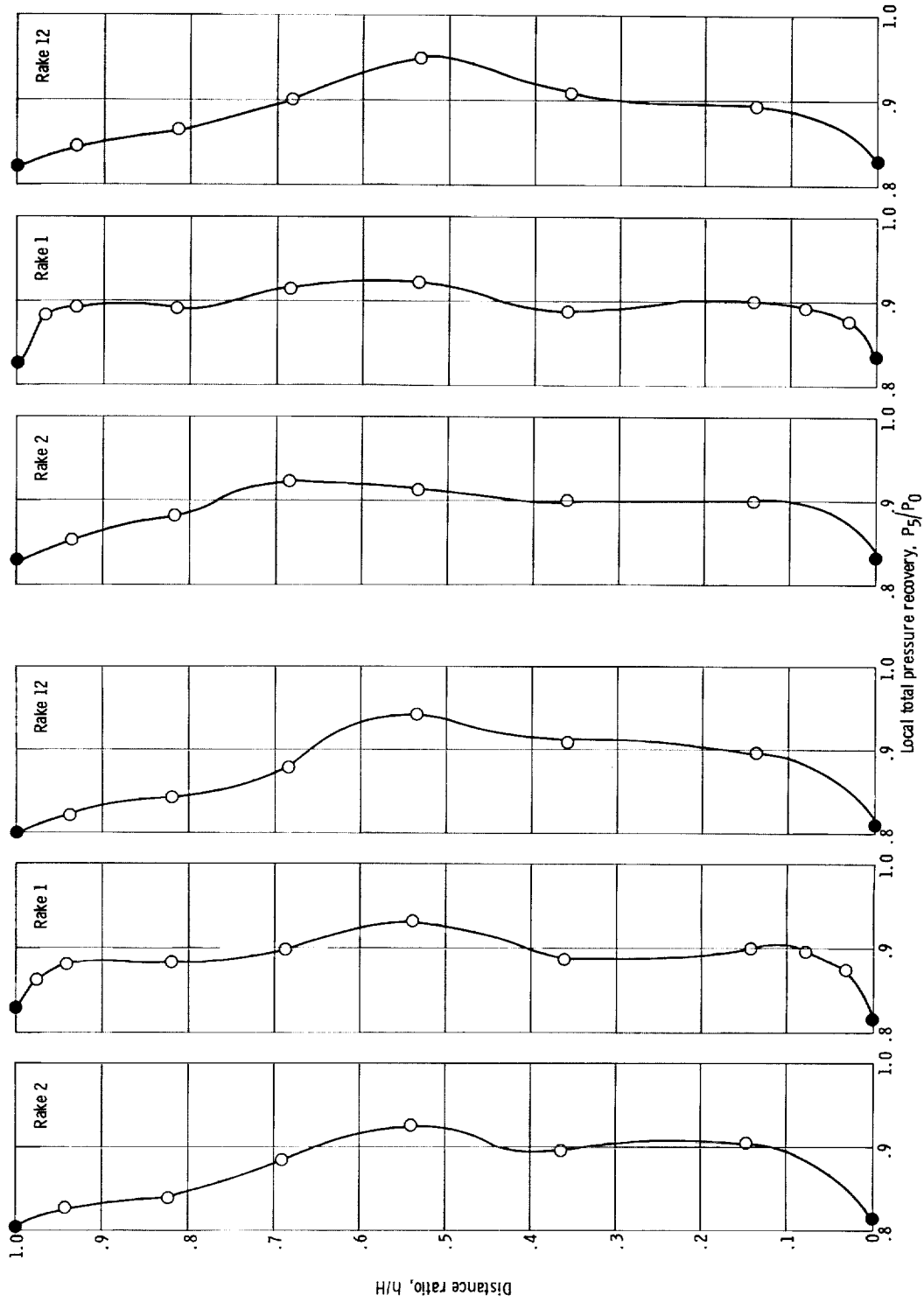


(d) Right quadrant.

(c) Bottom quadrant.

Figure 21. - Concluded.

Open symbols denote
total pressure
Solid symbols denote
static pressure



(a) Bypass mass-flow ratio, m_{by}/m_0 , 0.009; average pressure recovery, P_5/P_0 , 0.887.
(b) Bypass mass-flow ratio, m_{by}/m_0 , 0.068; average pressure recovery, P_5/P_0 , 0.893.

Figure 22. - Compressor face total pressure profiles for critical inlet operation and operating bypass system - top quadrant. Free-stream Mach number, 2.5; angle of attack, 0° ; cowl-lip-position parameter, θ_L , 26.4° ; bleed mass-flow ratio, m_{bl}/m_0 , 0.020.

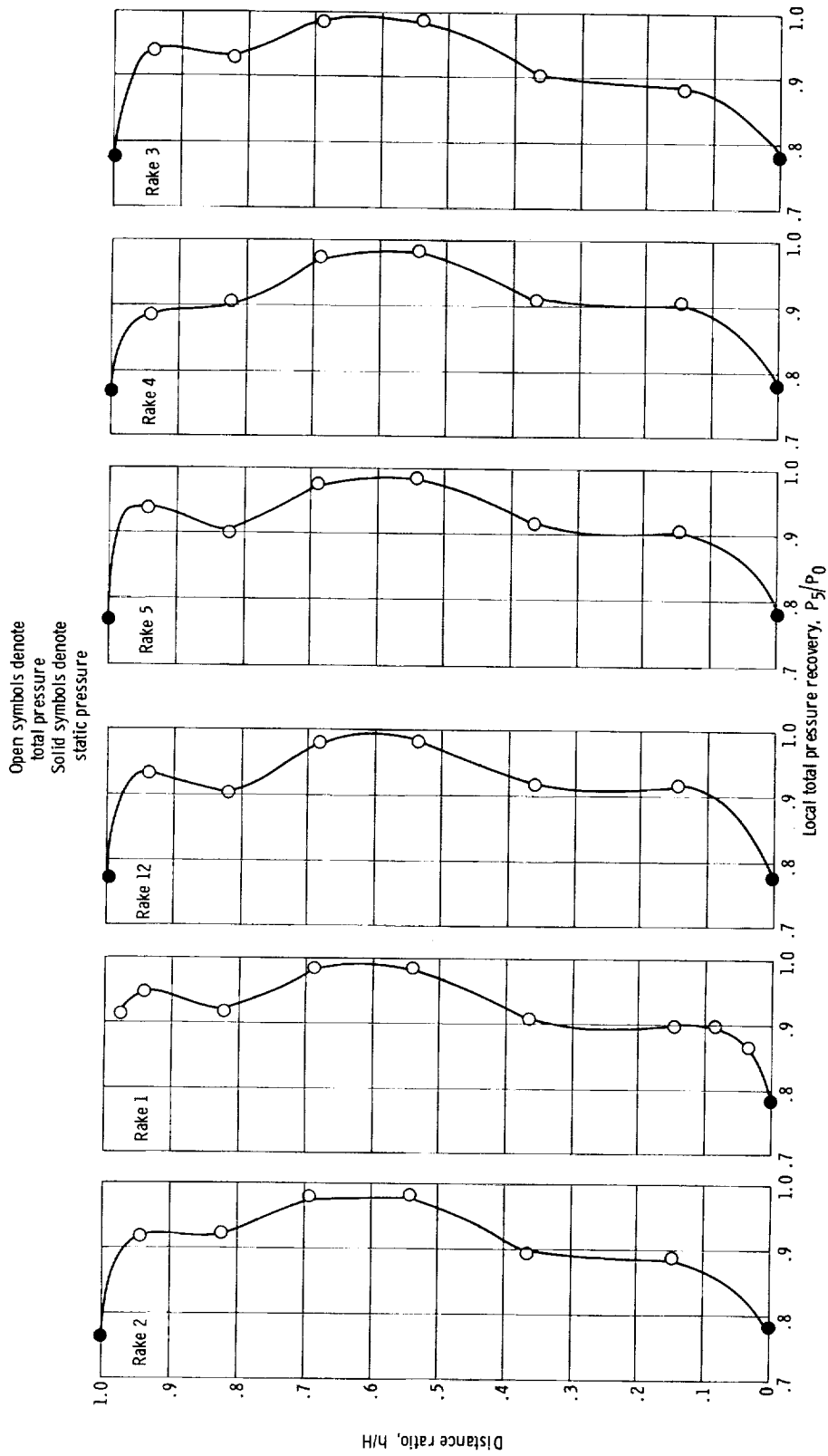
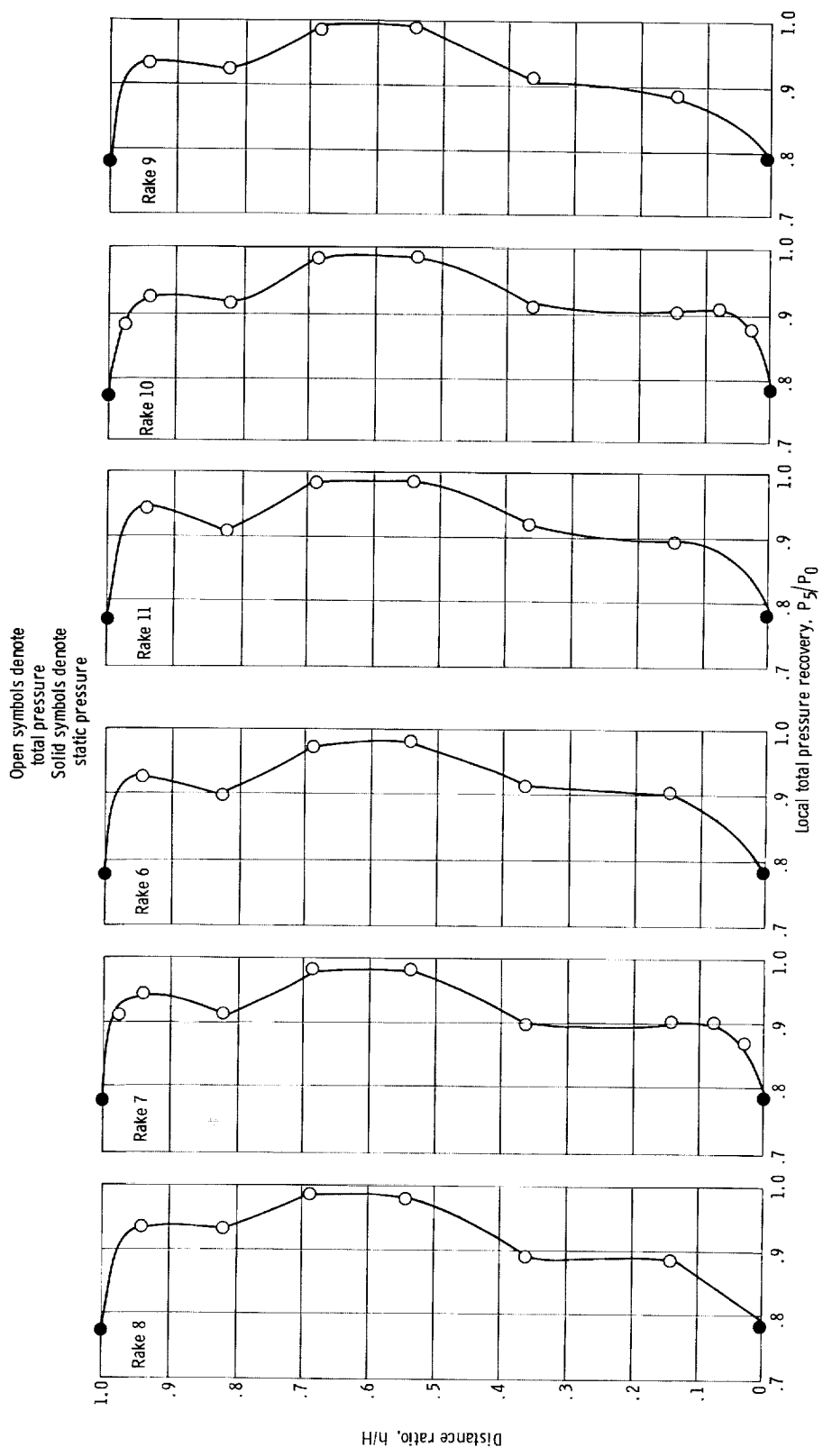


Figure 23. - Compressor face total pressure profiles for critical inlet operation and sealed bypass at free-stream Mach number of 2.0. Angle of attack, θ° ; cowl-lip-position parameter, θ_L ; $2\theta_L$; performance bleed, η_{bl}/m_0 ; 0.01 $\frac{3}{4}$; average pressure recovery, P_5/P_0 ; 0.938.



(d) Right quadrant.

(c) Bottom quadrant.

Figure 23. - Concluded.

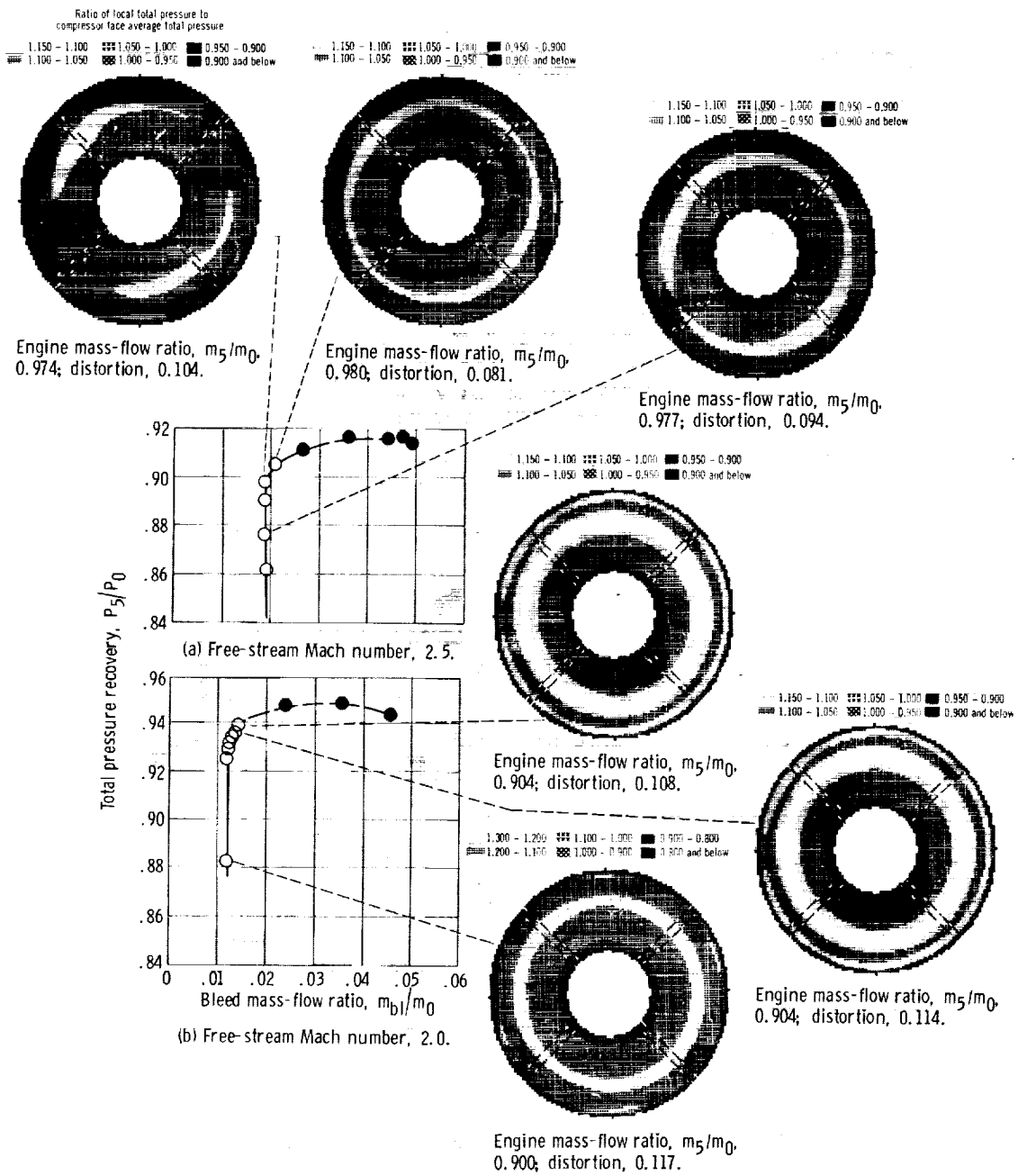


Figure 24. - Steady-state distortion profiles at free-stream Mach numbers of 2.0 and 2.5. Angle of attack, 0° ; cowl-lip-position parameter, θ_l , 26.4° ; sealed bypass.

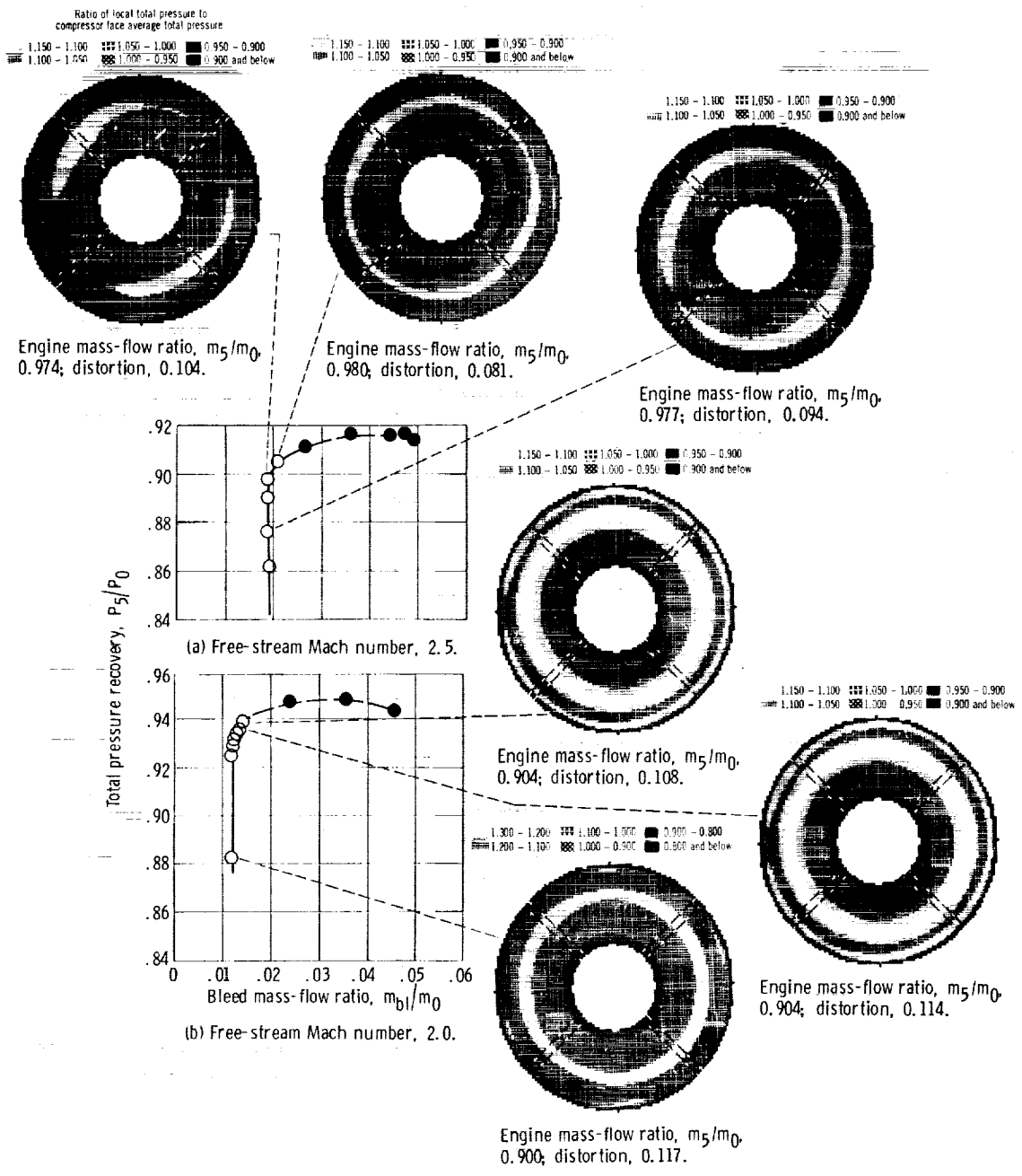


Figure 24. - Steady-state distortion profiles at free-stream Mach numbers of 2.0 and 2.5. Angle of attack, α^0 ; cowl-lip-position parameter, θ_l , 26.4^0 ; sealed bypass.

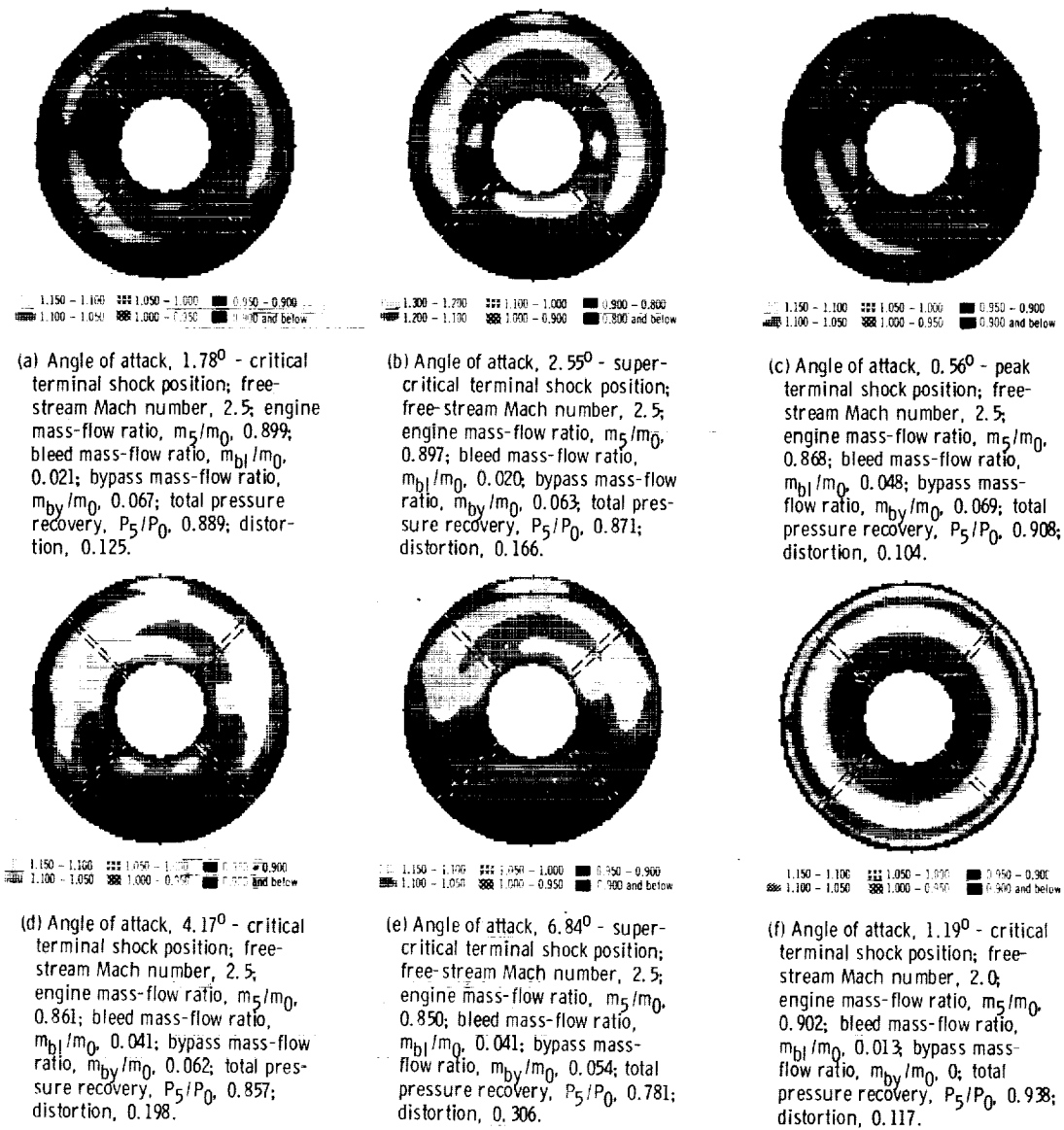
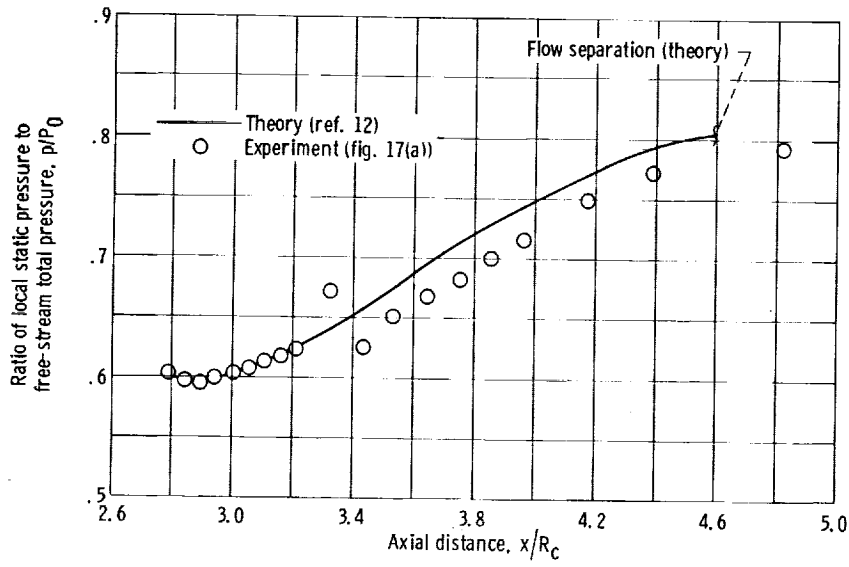
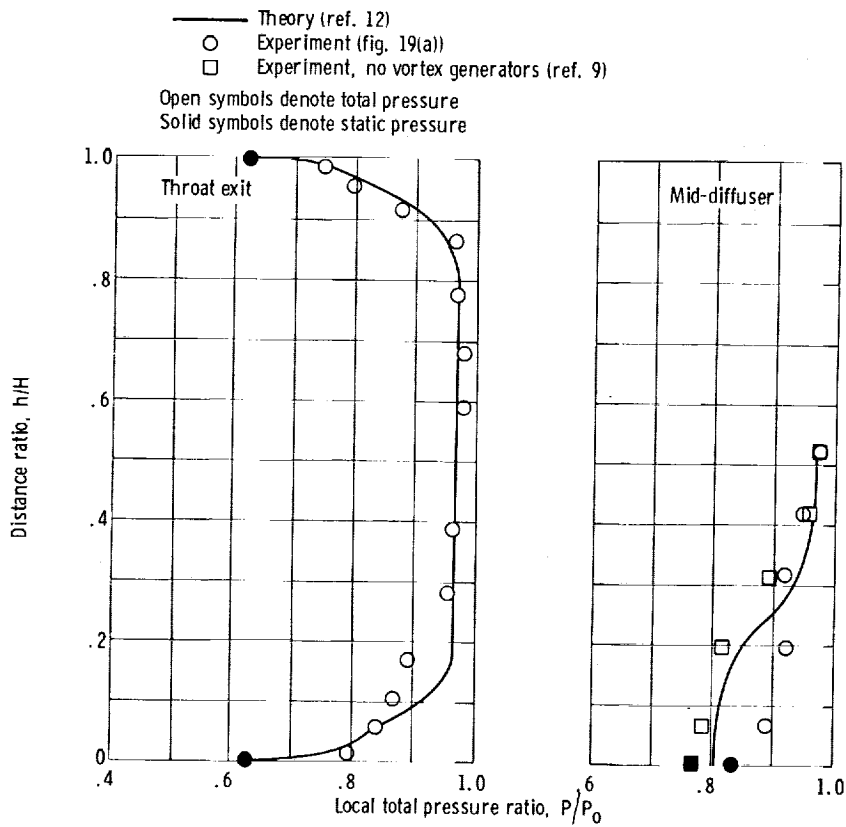


Figure 25. - Variation of steady-state distortion profiles at diffuser exit with angle of attack. Cowl-lip-position parameter, θ_L , 26.4° .



(a) Centerbody static pressure distribution.



(b) Diffuser rake total pressure profiles.

Figure 26. - Comparison of experimental and theoretical subsonic diffuser performance at peak inlet operation.

